Gait switches in deep-diving beaked whales: biomechanical strategies for long-duration dives

Lucía Martina Martín López[1], Patrick Miller[1], Natacha Aguilar de Soto[1,2], Mark Johnson[1]

[1] SMRU (Sea Mammal Research Unit), University of St. Andrews, Scotland

[2] BIOECOMAC (Biodiversidad, Ecología Marina y Conservación), Univesity of La Laguna, Tenerife, Spain

SUMMARY

Diving animals modulate their swimming gaits to promote locomotor efficiency and so enable longer, more productive dives. Beaked whales perform extremely long and deep foraging dives which likely exceed aerobic capacities for some species. Here, we use biomechanical data from suction-cup tags attached to three species of beaked whales (*Mesoplodon densirostris*, n=10, *Ziphius cavirostris*, n=9, and *Hyperoodon ampullatus*, n=2) to characterize their swimming gaits. In addition to continuous stroking and stroke-and-glide gaits described for other diving mammals, all whales produced occasional fluke-strokes with distinctly larger dorso-ventral acceleration, which we termed 'type-B' strokes. These high-power strokes occurred almost exclusively during deep dive ascents as part of a novel mixed gait. To quantify body rotations and specific acceleration generated during strokes we adapted a kinematic method combining data from two sensors in the tag. Body rotations estimated with high-rate magnetometer data were subtracted from accelerometer data to estimate the resulting surge and heave accelerations. Using this method we show that stroke duration, rotation angle and acceleration were bi-modal for these species, with B-strokes having 76% of the duration, 52% larger body rotation and 4 times more surge than normal strokes. The additional acceleration of B-strokes did not lead to faster ascents but rather enabled brief glides which may improve the overall efficiency of this gait. Their occurrence towards the end of long dives leads us to propose that B-strokes may recruit fast-twitch fibres that comprise ~80% of Blainville's beaked whales' swimming muscles, thus prolonging foraging time at depth.

Word count (246)

Keywords: biomechanics, swimming-gaits, magnetometer, accelerometer, beaked whales, deep diving

INTRODUCTION

Locomotor efficiency is critical for any active foraging animal but is especially so for animals that must travel long distances between resources (van Ginneken et al., 2005; de Knegt et al., 2007), such as breath hold divers who access oxygen at the sea surface and food at depth (Kramer, 1988). For these animals, reduced cost of transport increases the time and energy available for foraging (Williams, 1996). Numerous anatomical, behavioural and physiological factors influence the cost of transport for swimming animals including body shape (Williams, 1999), stroke frequency (Mori et al., 2010), speed (Aguilar de Soto et al., 2008), net buoyancy (Miller et al., 2012) and muscle type (Rome, 1992). These factors can vary over long time scales, e.g., due to ontogenetic (Noren et al., 2006) or body condition changes (Biuw et al., 2003; Mori et al., 2010), but some factors also vary within individual dives such as buoyancy forces which change with depth (Lovvorn and Jones, 1991).

Terrestrial animals modulate their locomotor power and speed by changing the rate and amplitude of propulsive motions, but also by changing their gait, i.e., the pattern of movements. Aquatic animals also exhibit gait changes: fish switch from pectoral to caudal locomotion (Webb, 1994a; Webb, 1994b) and squid from undulatory to jet propulsion (Webber and O'Dor, 1991; Svendsen et al., 2010). Most marine mammals use only a caudal propulsor while swimming, but they employ distinct stroking rhythms (i.e., continuous stroking, gliding, stroke-and-glide), analogous to gaits in terrestrial animals, to meet changing power requirements (Williams et al., 2000; Cook et al., 2010). Continuous stroking is used when high thrust levels are required; e.g., to counter strong positive buoyancy from air in the lungs when the animal dives away from the surface (Miller et al., 2004). Gliding is only possible when buoyancy forces are small or act in the direction of movement (Skrovan et al., 1999; Miller et al., 2004). At other times diving animals often use a stroke-and-glide gait. Despite the elevated drag associated with reacceleration between glides, this interrupted swimming has been estimated to save 15-50% of locomotor cost compared to steady swimming in fish (Weihs, 1974; Fish et al., 1991) and around 28% in Weddell seals (Williams et al., 2000).

In addition to using different swimming styles, aquatic animals modulate the amplitude and rate of strokes to change power output (Skrovan et al., 1999). Variations in stroke frequency and amplitude compensating for dynamics in buoyancy and drag have been recorded in turtles,

diving birds and marine mammals (Skrovan et al. 1999; Wilson and Liebsch, 2003; Hays et al. 2007). Faster and larger strokes are also used to produce bursts of speed for pursuit (Wilson and Liebsch, 2003; Aguilar de Soto et al., 2008) or escape, at least in fish (Blake, 2004). However, the usual stroking frequency in steady swimming aquatic animals follows a $mass^{-0.3}$ law over more than 4 orders of magnitude of body mass while usual swimming speed remains relatively constant at about 1.5 m/s (Sato et al., 2007). It has been suggested that there is an optimal size-related stroke frequency during diving that minimizes the cost of transport in seabirds (Mori et al. 2010). There may also be an optimal stroke amplitude as high-amplitude strokes produce more thrust (Fish et al., 2014) but also increase induced drag due to the greater flow disturbance of the extended propulsor (Fish et al., 1988).

For fish, the ability to swim with different gaits and stroke rates is closely connected with distinct types of muscle fibres optimized to different activity levels. Two fibre types are found in the musculature of fish (Jayne and Lauder, 1994): slow-twitch oxidative fibres (red muscle or Type I) are used for slow steady swimming, while fast-twitch fibres (white muscle or Type II) are recruited to power brief bursts of fast swimming during predator avoidance or prey capture (Alexander and Goldspink, 1977). Type I and II muscle fibres are also present in the swimming muscles of marine mammals but less is known about how these are employed (Kanatous et al., 2008, Velten et al., 2013). It is generally assumed that diving mammals minimise their reliance on anaerobic metabolism by choosing dive durations in keeping with their activity levels (Butler and Jones, 1997). The longest dive that an animal can make while relying primarily on oxygen stored in the blood and muscle is named the aerobic dive limit, ADL (Kooyman and Ponganis, 1998) or diving lactate threshold (Butler and Jones, 1997). The ADL for animals with the same oxygen store per unit mass should increase with body size (Martin and Smith, 1999; Halsey et al., 2006) due to lower mass-specific metabolic rates (White et al., 2009). However, 25000 kg sperm whales and 1000 kg beaked whales perform dives of comparable duration (30-50 min) and depth [600-1200 m, (Tyack et al., 2006; Watwood et al., 2006)], while more active 2500 kg pilot whales dive to similar depths but for substantially shorter intervals [15-20 min, (Aguilar de Soto et al., 2008)], raising the question of how the smaller beaked whales can dive for such long durations.

Beaked whales, a speciose family of deep diving toothed whales, have several anatomical structures including unnotched lunate flukes, a slender peduncle and small pectoral flippers that fit into depressions in the body wall (True, 1910; Mead, 1989) which seem to promote efficient swimming (Fish and Rohr, 1999). Like other deep-diving marine mammals, beaked whales also have physiological adaptations that prolong their ADL: high lipid volume density and myoglobin concentrations increase oxygen stores while extremely low mitochondrial volume densities and large fibre diameters reduce the metabolic rate (Velten et al., 2013; Davis, 2014). Nonetheless, it is likely that the two smallest ziphiid species studied to date, Cuvier's (*Ziphius cavirostris*) and Blainville's (*Mesoplodon densirostris*), routinely dive beyond their ADL, powering some portion of locomotion in deep dives anaerobically (Tyack et al., 2006; Velten et al., 2013). Despite this, both species make distinctive and enigmatic low-pitch ascents from deep dives. These ascents, which appear to be free of foraging, often take 2-3 times longer than descents (Tyack et al., 2006) suggesting a conservative slow swimming strategy. But rather than having the expected high percentage of slow-twitch oxidative fibres (Kanatous et al., 2002; Williams et al., 2011), the locomotor muscles of Blainville's beaked whales comprise about 80% fast-twitch fibres similar to those of sprinting athletes (Velten et al., 2013). The unusual combination of long dives and a predominance of anaerobic muscle, at least in the one species evaluated, makes beaked whales excellent candidates to explore how swimming gaits change in response to the progressive depletion of oxygen stores through the course of deep dives.

A prerequisite for understanding the biomechanical strategies of swimming animals is the quantification of stroke rate, amplitude and surge acceleration under varying load conditions. Underwater cameras, accelerometer and gyroscope tags have been used to study stroking in cetaceans, pinnipeds, turtles and diving birds (Williams et al., 2000; Wilson and Liebsch, 2003; Hays et al., 2007; Aguilar de Soto et al., 2008; Fossette et al., 2010). However, all three approaches have limitations. Cameras only capture the displacement of the propulsor, not the resulting body accelerations (Davis et al., 2001), while accelerometers are sensitive to both the orientation and the specific acceleration (i.e., the surge and heave acceleration) of the body (Fish et al., 2003). As stroking generates both specific acceleration and body rotations at the stroking rate, these two movement components cannot be quantified separately without additional sensors (Sato et al., 2007; Simon et al., 2012). Gyroscopes can provide independent information about

orientation, enabling estimation of the specific acceleration when combined with magnetometers and accelerometers, but the power consumption and drift of miniature gyroscopes (Noda et al., 2012) make them unattractive for animal biologging devices.

Here we investigate if and how beaked whales adapt their swimming gates throughout deep dives as oxygen stores are consumed. For this we adapt a method developed for human body tracking (Bonnet and Héliot, 2007) to separate body rotations and accelerations during stroking movements. The method requires two high-rate on-animal sensors that are already widely-used in tags: magnetometers and accelerometers. The new approach allows us to quantify simultaneously the rate, relative amplitude and surge acceleration of fluke-strokes. We use the method to examine the swimming movements of three ziphiids: Blainville's beaked whale (*Mesoplodon densirostris*, Md), Cuvier's beaked whale (Ziphius cavirostris, Zc), and northern bottlenose whale (*Hyperoodon ampullatus*, Ha), and show that all three species produce distinctive fast high-thrust fluke-strokes intermixed with normal strokes during ascents from deep dives. The additional acceleration generated by fast strokes do not seem to lead to shorter ascents (i.e., with higher pitch or speed) but result in brief glides that may enable muscle recovery while reducing the average drag, possibly improving overall energetic efficiency when compared to continuous stroking.

RESULTS

A total of 118, 96, and 16 hours of tag recordings from 10 Md (7 individual whales), 9 Zc and 2 Ha were analysed containing 49, 43 and 6 deep dives, respectively. Unresolved tag moves on the body of the whale led to 9 dives being removed from analysis. At least two entire deep dives were recorded from each whale (Table 1). As described elsewhere (Hooker and Baird, 1999; Baird et al., 2006; Tyack et al., 2006, Arranz et al., 2011), these beaked whales typically perform long deep foraging dives (Md: means of 49 min and 844 m; Zc: 59 min and 1044 m; Ha: 49 min and 1572 m in the data analysed here). For Md and Zc, ascents from deep dives were about twice as long in duration as descents and were performed at proportionally lower vertical speeds and absolute pitch angles (Table 1). Because of the typically low pitch angle, forward speed could not be estimated accurately throughout ascents but in the few intervals with higher pitch angle, the forward speed was about the same in ascents and descents suggesting that the

long ascents are a result of the low pitch angle rather than slow swimming (Tyack et al., 2006). The situation is different for Ha: the pitch angle of descents and ascents is similar for this species but swimming is slower during ascent leading to a smaller but still significant difference in duration.

Stroke and glide patterns

Tagged whales stroked continuously in the initial part of descents presumably to overcome the buoyancy of gases carried from the surface (Fig. 1) (Miller et al., 2004; Simon et al., 2009, Simon et al., 2012). Stroking was continuous until a mean depth of 128 m (Md), 197 m (Zc), and 95 m (Ha). The remainder of the descents were performed with prolonged glides and occasional bursts of stroking or stroke-and-glide. On ascents, terminal glides began at depths of 30 m (Md), 34 m (Zc), and 36 m (Ha). Below this, the gait varied from continuous stroking to stroke-and-glide with some strokes having distinctly larger peak high-pass filtered dorso-ventral acceleration, $\tilde{a}_{zt}$ (Fig.1). These high acceleration strokes were typically performed singly and followed by a short glide. However, there were occasional bursts of up to 3, 14 and 2 consecutive of these high-acceleration strokes in Md, Zc and Ha respectively. The consistent presence of these high acceleration strokes during ascents but not descents for all three species of beaked whales (Fig. 2) led us to investigate their occurrence and characteristics. Because the accelerometer output is affected by both body rotations and specific acceleration, the increased high-frequency dorso-ventral acceleration in these strokes could result from a larger stroking amplitude or a faster stroke, or both.

To examine separately the contribution of specific acceleration and body rotation in Md and Zc, we first used the magnetometer method to estimate body rotations, r_t, and then combined this with the accelerometer data to estimate the heave and surge accelerations. As asymmetric strokes were often encountered in these signals, we analysed half-strokes defined as the intervals between successive zero-crossings in the estimated body rotations, $\hat{r}_t$. This signal, being insensitive to acceleration, is relatively smooth (Fig. 3) and so half-strokes can be reliably detected and measured.

Each half stroke was parameterized by the RMS value of the rotation, and the surge, heave, and $\tilde{a}_{zt}$ over the interval. Plots of these parameters as a function of half-stroke duration

(Fig. 4) show two clearly separated clusters indicating that the observed gait variations during the ascent correspond to distinct stroke types rather than a continuum of strokes with varying parameters. These plots indicate that the high acceleration strokes noted in Fig. 2 also have consistently shorter duration and we refer to these short-strong strokes as 'type-B' strokes in the following to distinguish them from the more numerous 'normal strokes'. As the RMS heave acceleration typically showed the clearest bimodality, we used a threshold in this parameter to distinguish normal and B-strokes. To account for different tag placements, the threshold was selected separately for each animal from a histogram of RMS heave acceleration (Table 2). While normal up- and down-strokes had similar accelerations and body rotations, up and down B-strokes, were often asymmetric (Fig. 4) although the relative magnitude of stroke parameters in each half stroke varied with animal presumably as a result of different tag placements. Accordingly, we report the average over all half-strokes when comparing parameters between normal and B-strokes in the following.

Because the tags used on *Hyperoodon* lacked a high-rate magnetometer, a different method was needed to distinguish strokes in this species. Half-strokes were identified from zero-crossings in $\tilde{a}_{zt}$. Although wide hysteretic thresholds were used to avoid detecting multiple zero-crossings due to transient accelerations, the resulting half-stroke durations are more variable for this species than for Md and Zc indicating that there are likely frequent errors in stroke detection. Nonetheless, reasonably distinct clusters corresponding to the two stroke types during ascents appear in plots of RMS $\tilde{a}_{zt}$ versus duration and a $\tilde{a}_{zt}$ threshold was used to separate normal and B-strokes (Table 2).

Stroke parameters

The three species spend more time gliding over the 100 to 400 m range in descents vs ascents (Md mean of 5.6 min vs 2.2 min desc/asc; Zc 9.1 vs 3.3; Ha 6.8 vs 4.5; see Table 1 for s.d). Counting both stroke types, Md and Ha produced about 2 to 3 times as many half-strokes to ascend over this depth range than to descend (Md mean of 0.23 vs 0.57 strokes/vertical meter desc/asc; Ha 0.11 vs 0.21). For *Ziphius* the stroke counts were more balanced (0.31 vs 0.27 desc/asc) with some individuals stroking more in descents than in ascents. For the shallow ascents of Md and Zc more strokes are expected to cover the 300 meters depth range. But even

considering this, there are still more ascent strokes per meter for Md (mean of 0.20 vs 0.30 desc/asc) while for Zc the effort made to ascend is less than to descend (mean of 0.29 vs 0.17 desc/asc). The mean duration of normal half-strokes was 1.1 and 1.4 s for Md and Zc, respectively, implying stroking rates in normal continuous swimming of 0.44 (Md) and 0.36 (Zc) Hz. B half-strokes identified during the ascent phase of deep dives had a mean duration of 76% (averaging up- and down-strokes) of normal half-strokes in Md and Zc implying a 30% increase in the instantaneous stroking rate. Body rotation was also larger for B-strokes by about 52% and the high-frequency dorso-ventral acceleration as well as the estimated surge and heave accelerations were 2.5-4 times larger in B-strokes as compared to normal strokes (Table 2). These ratios were surprisingly stable across individuals and between the two species. For *Hyperoodon*, normal half-stroke duration was 1.6 s giving a stroking rate of 0.32 Hz (Table 1). For Ha, the duration of B half-strokes was 70% that of normal strokes while the dorso-ventral acceleration was 2.5 times higher in B-strokes.

Given the 4 times increase in estimated surge acceleration for B-strokes in Md and Zc, there should be a corresponding increase in forward speed during these strokes. Unfortunately, the ascent pitch angle of these species was usually too low to allow forward speed estimation from vertical speed. However, forward speed could be estimated during some brief episodes of steep ascent in one Zc (Fig. 5). For this animal, there was a significant difference in the speed increment over two consecutive B-strokes compared to two normal strokes (t-test p-value <0.0001). Consistent with the increased thrust, each burst of 2 B-strokes produced a speed increment of 0.5 ± 0.1 m/s accelerating the animal to speeds of 1.7-2 m/s, while pairs of normal strokes produced no speed increment (0.0 ± 0.10 m/s). Thus in Fig. 5, the long bout of normal strokes only produced sufficient thrust to maintain a steady forward speed of 1.3 m/s.

Occurrence of B-strokes

While normal strokes were present in all descents and ascents of deep and shallow dives, gait switches to and from B-strokes occurred almost exclusively in deep-dive ascents. B-strokes were detected in 42 of 49 deep dive ascents of *Mesoplodon*, 37 of 43 for *Ziphius* and 5 of 6 for *Hyperoodon*, and comprised an average of 30% of the ascent strokes in Md and Ha and almost 50% in Zc (Table 1). B-strokes were also identified in the ascent phase of 5 out of 104 shallow

dives performed right after a deep dive. *Mesoplodon* foraging dives without B-strokes (n=7) were performed by two different whales and were amongst the shortest deep dives recorded (37.7±7.3 minutes cf. overall mean of 49±5; mean ± S.D.). The 6 *Ziphius* deep dives without B-strokes were performed by three different whales and were also relatively short (43.3±5.9 min. cf. overall mean of 59±12; mean ± S.D.). The only *Hyperoodon* deep dive without B-strokes, however, was not short (52 min cf. 49±4 mins; mean ± S.D.).

To explore the possibility that B-strokes were associated with longer, faster or more vertical swimming we used a generalized linear model relating stroke presence to time and vertical speed (see Appendix section A3). Because time into dive appeared to have a significant effect on the presence of B-strokes in all three species, we compared the actual occurrence of B-strokes in ascents to a model which allocated the same number of B-strokes at random throughout the ascent. B-strokes began during the ascent at mean times of 34 min (Md), 44 min (Zc) and 35 min (Ha) well after the mean start of ascent times of 30 min (Md), 38 min (Zc) and 31 min (Ha). In each species, B-strokes appeared significantly later than expected by the random model. Although B-strokes tended to co-occur with higher vertical speed, this factor explained little of the variability in stroking. Thus, the 4 times increase in surge acceleration during B-strokes does not translate consistently into a commensurate increase in ascent speed. This seems to be a consequence of the frequent co-occurrence of B-strokes with glides. Taken as a unit, B-strokes and glides involve similar average activity as continuous stroking (Table 2; Appendix section A3). Although distinct gait switches were not evident in acceleration signals during descents, 0-16% of B-strokes detected using the heave acceleration threshold occurred during deep-dive descents in Md and Zc. About 66% of these occurred in the first 100 meters of the descent where high accelerations are needed to overcome buoyancy due to air in the lungs (Miller et al., 2004). The duration and rotation magnitude of B-strokes were similar for descents and ascents, but the heave and surge accelerations were smaller (approx. 50-80% of their ascent values, inferred from Table 2).

DISCUSSION

Natural selection on breath-hold divers should favour adaptations that reduce the cost of transport and thereby increase the time and energy available for foraging at depth (Williams,

1996); one such adaptation would be to choose gaits that are efficient given the changing physiological and mechanical constraints throughout a dive (Alexander, 2003; Mori et al., 2010). Here, we examined the swimming gaits employed by three beaked whale species with similar morphology and diving patterns, but a 7:1 range of adult body masses (Silva and Downing, 1995; Allen et al., 2011a; Allen et al., 2011b). All three species produced a previously un-described stroke-and-glide gait involving two distinct types of strokes that occurred primarily during ascents from deep dives: the normal locomotory stroke and a faster, more energetic stroke which we term B-stroke (Figs 2, 3). Type-B strokes had 2.5 times more dorso-ventral high-frequency acceleration than normal strokes (Table 2) and so were readily detected in on-animal accelerometer data (Fig. 2). But because accelerometers are influenced by both body rotations and specific acceleration, the increased acceleration could have resulted from either a larger stroke amplitude or a faster stroke, or both. To distinguish between these possible drivers of the acceleration signal, we combined high-resolution accelerometer and magnetometer signals to separately quantify body rotations and specific accelerations during stroking (Bonnet and Héliot, 2007). Using this method we confirmed that B-strokes are distinct from normal strokes in terms of duration and body rotation, as well as surge and heave acceleration. We also found that B-strokes often precede short glides which are presumably enabled by the increased thrust of this stroke.

Due to the difficulty of encountering and tagging beaked whales, the sample size of individual animals is relatively small. However, the consistent presence of B-strokes in all tagged animals from three species suggests that this locomotion pattern may be a common component of ziphiid diving behaviour. In the following we first discuss the magnetometer-method and its limitations and then consider what role the observed gait switching may play in the diving strategy of beaked whales.

Magnetometer: a detailed insight into swimming gaits

Magnetometers are commonly employed in tags to estimate heading and are generally sampled at a low rate to minimize power consumption. Adapting the method of Bonnet and Héliot (2007), we demonstrated that high sampling rate on-animal magnetometer data can be used also to determine body rotations during stroking. Triaxial magnetometers are a vector

sensor like accelerometers and so can be used to deduce two components of the instantaneous orientation of an animal but, unlike accelerometers, they are not sensitive to specific acceleration. This means that for relatively simple motions like swimming in which the rotations largely occur in a single plane, the instantaneous orientation of the animal can be estimated solely from the magnetometer. By combining these body rotation estimates with simultaneously-sampled high-resolution accelerometer data, the orientation and specific acceleration components in the accelerometer can be separated enabling a detailed analysis of stroking styles. Although several simplifying assumptions are required for this method, the single plane movement model appears to be a good approximation for ascent and descent swimming in Md and Zc (see Appendix section A1). An additional advantage of using magnetometers to study stroking is that stroke duration can be measured more precisely with this sensor than with an accelerometer. This is because the body rotations measured by a magnetometer vary relatively smoothly due to the rotational inertia, i.e., the resistance to angular acceleration, of the animal. In comparison, the $\tilde{a}_{zt}$ accelerometer signal can have substantial high frequency transients making it more difficult to identify individual strokes reliably (Fig. 3).

The method developed here can be modified for other swimming fauna provided that the locomotion oscillation occurs mostly in one plane (e.g., for seals and caudally-propelled fish, it would be a yaw rotation rather than a pitch). There are, however, some limitations to the method. Because of the assumption that low frequency components in the accelerometer are entirely due to orientation changes, only the dynamic forces during stroking can be estimated. Thus slowly-changing forces such as mean drag, lift and buoyancy cannot be estimated. Secondly, as with accelerometers, body rotations will not be observed by a magnetometer if the animal is swimming such that the axis of rotation is parallel with the field vector. These body orientations were rare in our data (<3.3% of Md and Zc analysed dive time) but could be more prevalent at low latitudes where the magnetic field vector is nearly horizontal. Finally, a limitation with all tagging methods is that measurements are only made at one location on the animal, making it difficult to predict how other parts of the body are moving. Stroke duration and therefore stroking rate are not affected by tag location but the magnitude of rotations, specific accelerations and the mechanical events analysed as up or down-strokes are. To overcome this sensitivity, we calculated the ratio of stroke body rotations and specific acceleration between

normal and B-strokes, in effect normalizing these parameters of B-strokes to the values in normal strokes. These ratios appear to be fairly stable across individuals and/or tag locations within each species but are even broadly similar across Md and Zc (Table 2). This suggests that the proportional increase in acceleration and rotation due to the gait switch may be a fundamental aspect of the movement that is dictated more by anatomical structures than behavioural decisions.

Different strokes:

The magnetometer method provides detailed information about the two different stroke types produced by beaked whales during deep-dive ascents. For the two species (Md and Zc) that could be analysed with this method, type-B half strokes were some 76% of the duration of normal strokes and had 52% greater rotation. Assuming that body displacement is proportional to rotation, the heave acceleration should therefore increase 2.6 times (i.e., displacement x rate^2 = $1.52/0.76^2$) under a sinusoidal movement model. Actual RMS heave accelerations estimated using the magnetometer method were a mean of 3.1 (Md) and 3.5 (Zc) times larger in B-strokes as compared to normal strokes (Table 2) indicating that B-strokes are consistently more energetic than expected by simply scaling normal strokes. Surge accelerations are also greatly increased in B-strokes compared to normal strokes (mean increase of 4 times for Md and Zc) and the waveforms for both accelerations (Fig. 6C) show short high-magnitude transients in B-strokes that are largely absent in the more sinusoidal signals of normal strokes.

Thus, B-strokes not only utilize increased speed and amplitude of propulsor motion but are also performed more abruptly than in normal swimming leading to the production of brief but powerful bursts of thrust. These bursts translated directly into increased forward speed in the one Zc that ascended steeply enough to allow reliable forward speed estimation (Fig. 5). While continuous normal strokes generated sufficient thrust to maintain a speed of some 1.3 m/s, pairs of B-strokes rapidly accelerated the animal to 1.7 m/s. However, over longer time intervals, B-strokes did not lead to substantially increased forward speed as evidenced by the weak explanatory power of a model matching speed to presence of B-strokes in 10 s (Md) or 15 s (Zc and Ha) intervals. This is because individual short bursts of B-strokes were typically followed by

glides with duration equivalent to 2-3.5 normal strokes as in Fig. 5. In comparison, normal strokes generally occurred in prolonged bouts and so were seldom followed by a glide.

Averaging over the full gait unit, B-strokes and glides produced about as much force per unit time as continuous normal stroking (VeDBA in Table 2). Thus, the extra thrust of B-strokes facilitates a lower stroking duty-cycle in ascents rather than faster swimming. Although by far the majority of B-strokes occurred in ascents from deep dives, a small proportion of descents strokes were also categorized as B-strokes using a heave acceleration threshold. These descent B-strokes did not occur with glides but most occurred in the first 100 m of descent where continuous stroking may be needed to counter positive buoyancy from air in the lungs. This energetic stroking style thus appears to be utilized in two ways: (i) as a low-duty cycle alternative to normal stroking, and (ii) as a high thrust gait to overcome strong forces. A third use may be to accelerate animals when escaping predators or pursuing prey although this behaviour was not observed in the data analysed here. But while the biomechanical advantage of a high acceleration stroke in initial descents, prey chase and predator avoidance is evident, the benefit of using this gait in ascents is less clear. Nonetheless, the B-stroke-and-glide gait powers some 53% of vertical travel in ascents of all three species, making it an important component of transport. Preferential use of this gait would be understandable if it is energetically more efficient than continuous normal stroking but, in which case, why would it not be used for most or all transport locomotion? Two different modelling approaches show a weak but significant trend for this gait to be used later in dives suggesting that it replaces continuous stroking as oxygen stores dwindle rather than offering an efficient alternative throughout dives. This is supported by the observation that the few ascents performed without B-strokes by Md and Zc are among the shortest dives in our data. To explore this further, we compare the diving behaviour of the three beaked whale species.

Different diving strategies

As body size increases, oxygen stores increase relative to metabolic rate, other factors being equal (Martin and Smith, 1999; Halsey et al., 2006). Although the metabolic cost of diving depends upon a number of factors in addition to body mass, there should be sizeable differences in the diving capabilities of the beaked whale species studied here. The overall diving pattern of

the three species is broadly similar comprising long deep foraging dives interspersed with sequences of shallow dives with no apparent foraging (Hooker and Baird, 1999; Tyack et al., 2006). However, the durations of deep dives do not show the expected variation with body mass (Table 1). *Hyperoodon* with 7 times the mass of *Mesoplodon* performed similar duration dives (mean of 49 mins) in our data albeit to almost twice the depth (Table 1). *Ziphius* made consistently longer dives (mean of 59 mins) than recorded for Md and Ha but to intermediate depths of about 1000 m, although dives to 3000 m have been reported for this species (Schorr et al., 2014). Despite these disproportionate dive durations, all three species perform B-strokes in most (84 of 98) deep dive ascents. The swimming speed and distance covered in dives also contribute to the metabolic cost. *Mesoplodon densirostris,* the smallest of the three species, ascend at one half the vertical speed of descents primarily due to a halving of the pitch angle. Neglecting lift, these long shallow ascents cover roughly 75% more distance over the 100-400 m depth range than descents and require 2.5 times more strokes (Table 1) indicating a body density greater than water. *Ziphius cavirostris* also ascend at low pitch angle but use about the same number of strokes to ascend as to descend suggesting a more neutral body density. *Hyperoodon ampullatus* descend and ascend at high pitch angles in the limited data available but ascents take 20% longer and require 2 times more strokes than descents over the 100-400 m depth range suggesting a dense negatively buoyant body (Table 1). This simple analysis indicates two overlapping distinctions between these ziphiid species: body density and ascent angle. Low-pitch ascents reduce the thrust required per stroke to counter negative buoyancy (Gleiss et al., 2011b) permitting a lower propulsive power albeit for longer duration, and this may be the strategy adopted by Md. In comparison, the greater oxygen stores in dense-bodied Ha appear to be expended in powerful steep ascents that reduce transport-time and may enable access to deeper resources. The more neutral body of Zc compared to Md may lower the overall cost of transport (Sato et al., 2013) in this species enabling, in concert with the larger body size, the longer and deeper foraging dives. However, the shallow ascents in Zc are less easy to explain biomechanically and this behaviour in both Md and Zc may actually be a predator avoidance tactic in which animals invest energy in ascents to move away from the last point at which they vocalize (Tyack et al., 2006; Aguilar de Soto et al., 2012). If so, this crypsis must be obtained at the cost of reduced foraging time. In practice, a number of evolutionary forces may have

contributed to the diverse diving behaviour of these species. However, irrespective of the specific drivers, all three species have substantial propulsive needs in the last part of deep dives: to power long shallow ascents in Md and Zc, and to drive steep fast ascents in Ha. These calls on metabolic resources when oxygen stores are nearly depleted coincide with the appearance of B-strokes and lead us to question what benefits this specialized high acceleration gait may offer.

Gait switches and fast twitches?

Although stroke-and-glide gaits have been reported for a number of marine mammals, this is the first observation of a distinct stroke type within such a gait. This may be partly a consequence of sensor sampling rate as the wide bandwidth accelerometers (e.g., >10 times the stroking rate) required to reliably detect B-strokes have only been used relatively recently. However, high acceleration strokes have not been reported for other deep diving toothed whales tagged with the same devices as used here (Miller et al., 2004, Aguilar de Soto et al., 2008) suggesting that the routine production of B-switches may be peculiar to beaked whales. If so, it is surprising to find such energetic stroking in animals that rely on long deep foraging dives and would therefore be expected to adopt a conservative swimming style.

The high acceleration strokes described here have some 76% of the duration and involve a 52% larger body rotation than normal strokes implying a faster and larger amplitude movement of the flukes. To achieve this, the rate of muscle contraction must be doubled (i.e., 1.52/0.76) in B-strokes compared to normal strokes if the relationship between fluke extension and body rotation at the tag location is the same for both stroke types. This in turn implies a substantial increase in the metabolic cost of B-strokes which may be further exacerbated by a larger active drag due to the increased propulsor amplitude (Weihs, 1974). However, the increased thrust of B-strokes also enables short glides resulting in some 70% reduction in stroking duty cycle while maintaining roughly the same average speed in ascents. The lower stroke rate and reduced drag in glides will offset the cost of B-strokes but it seems unlikely that B-strokes are more efficient than continuous normal stroking, at least when muscles are well oxygenated, given the near absence of this gait early in dives and even throughout some short deep-dives by Md and Zc.

Information about muscle type and myoglobin concentrations are missing for most ziphiids but a recent anatomical study of *Mesoplodon densirostris* revealed an unexpectedly high

449 percentage, about 80%, of fast-twitch fibres in locomotor muscles (Velten et al., 2013). Although
450 these fibres may power bursts of high speed swimming, e.g., when escaping predators or chasing
451 prey, the authors propose that the primary function of Type II fibres during dives is not to power
452 locomotion directly, but to provide a large, metabolically inexpensive oxygen store within the
453 locomotor muscle, supplying oxygen to Type I fibres during routine swimming. But if swimming
454 in foraging dives only used Type I fibres then there is no reason to expect the strongly bimodal
455 stroking reported here. Rather, stroke rate and amplitude could be adjusted continuously within
456 the capabilities of these fibres to meet locomotion requirements (Johnson et al., 1994).
457 If the fibre composition reported for Md does have a connection with the B-stroke-and-
458 glide gait reported here, then a possible explanation is that Type II muscle fibres are recruited to
459 supplement propulsion when oxygen stores in Type I fibres are low, and the resulting faster
460 contraction rates of Type II fibres produce B-strokes. Similar fast-twitch recruitment when
461 muscles are fatigued has been observed in exercising humans (Houtman et al., 2013). This
462 hypothesis is supported by the strong bimodality in the stroke types and the disproportionately
463 high accelerations generated in B-strokes, both of which suggest that these high energy strokes
464 are produced in a way that is biomechanically distinct from normal strokes. If this interpretation
465 is correct, the short glides accompanying B-strokes may serve to maintain an average speed close
466 to the minimum cost of transport while also reducing drag (Fish et al., 1988). However, the
467 connection between muscle recruitment and movement is generally complicated (Jayne and
468 Lauder, 1994; Flammang and Lauder, 2008) and it is unlikely that there are simple one-to-one
469 relationships between muscle types and specific movement modes. Moreover, our biomechanical
470 interpretation of fibre function and the physiological function inferred by Velten et al. (2013) are
471 not mutually exclusive: the large resource of Type II fibres in Blainville's beaked whales could
472 provide both an oxygen store during most of the dive and an anaerobic power source when
473 oxygen stores dwindle. But if B-strokes do result from recruitment of fast-twitch fibres then our
474 data indicate that at least 3 species of beaked whales rely on anaerobic metabolism to power
475 swimming in most deep dive ascents. This strategy may enable both a long foraging phase and a
476 slow ascent as in *Mesoplodon* and *Ziphius* or a fast powerful ascent for *Hyperoodon*. In either
477 case, recruitment of anaerobic muscles must necessitate a post-dive recovery interval to process
478 lactate, and this may help explain the prolonged periods between deep dives reported for the

beaked whale species studied here (Hooker and Baird, 1999; Tyack et al., 2006). Thus this strategy comes at the cost of a lower time available for foraging: although many other factors influence diving rates, the proportion of time spent actively searching for prey on a daily basis by beaked whales [17-25% (Tyack et al., 2006; Arranz et al., 2011)] is well below that of sperm whales [53% (Watwood et al., 2006)].

Recruitment of different fibre types to produce diverse swimming gaits has been well documented in fish (Jayne and Lauder, 1994) with anaerobic pathways generally being reserved for predator avoidance or prey capture rather than routine transport (Alexander and Goldspink, 1977). Though we did not measure muscle fibre contractions directly, the results presented here are consistent with a process whereby anaerobic fibres are employed for routine locomotion by some extreme diving mammals to prolong foraging at depth. The observation that marine mammals can utilise strokes with substantially different mechanical output and energetic cost has an important bearing on methods used to assess locomotor cost. If animals produce a diversity of strokes, the number of strokes alone may be insufficient to characterize the cost of transport (Williams et al., 2004) and a method that takes into account either the duration of individual strokes or the acceleration [e.g., OBDA, (Wilson et al., 2006)] may be more accurate.

MATERIAL AND METHODS

Field site and study animals

Tagging was conducted on three beaked whale species: 10 Md were tagged from 2003-2010 off the island of El Hierro in the Canary Islands, Spain; 9 Zc were tagged from 2003-2008 in the Ligurian Sea, Italy; 2 Ha were tagged in 2011 in the Gully, Canada. Some Md were tagged unintentionally more than once due to the difficulty in recognizing individuals at the moment of tagging, resulting in tag deployments on 7 different whales (Table 2). *Mesoplodon* and *Ziphius* were tagged with DTag sound and movement recording tags following the methods described by Madsen et al., (2005). The tag dimensions were 20x10x3 cm giving a flow cross-section << 1% of the frontal area of Md and Zc. Tags were attached with four 6 cm diameter suction cups, minimizing the relative movement of the sensors with respect to the whale. The tag included sensors for pressure, triaxial acceleration and triaxial magnetism. All sensor channels were anti-aliased filtered with a single pole filter at 5 Hz before sampling at 50 Hz. Data were then

509 decimated in post-processing to a 25 Hz sampling rate using identical low-pass filters (10 Hz
510 cut-off frequency) on each sensor channel. *Hyperoodon* were tagged with single suction cup
511 Little Leonardo tags (W2000-3MPD3GT, 17.5 cm long x 3.0 cm diameter) following the data
512 collection methods described in Aoki et al. (2012). These tags recorded pressure, swim speed,
513 temperature and three axis magnetic field at a sampling rate of 1 Hz, and three axis
514 accelerometer data at 32 Hz. No anti-alias filter was present in the Little Leonardo tags.
515
516 **Dive types and phases**
517 Beaked whales perform long deep foraging dives interspersed with protracted intervals of
518 shorter shallow dives (Hooker and Baird, 1999) which do not appear to include foraging, at least
519 in Md and Zc (Tyack et al., 2006). As a result, the dive-depth histogram for each species is
520 bimodal with clearly separated shallow and deep dives. Using these separations, we defined deep
521 dives as those with maximum depth greater than 350 m, 600 m and 800 m for Md, Zc and Ha,
522 respectively.
523 The accelerometer and magnetometer signals recorded by the DTags and Little Leonardo
524 tags were corrected for the orientation of the tag on the whale, which was estimated at each
525 surfacing from the stereotypical movements during respiration (Zimmer et al., 2005). Suction
526 cup tags occasionally move on the animal; if a tag was found to have moved during a dive and
527 the time of the move could not be determined from the data, that dive was excluded from further
528 analysis.
529 Cetaceans propel themselves with dorso-ventral oscillations of their flukes which
530 generate surge and heave accelerations (i.e., specific acceleration in the longitudinal, and dorso-
531 ventral axes respectively), as well as body rotations (Fish et al., 2003). All of these movements
532 appear as cyclical variations at the stroking rate in accelerometer signals recorded on a
533 swimming whale and are overlaid on the constantly changing postural orientation as the animal
534 manoeuvres (Johnson and Tyack 2003; Sato et al., 2007). In steady swimming, an animal's
535 overall body posture varies slowly in comparison with the stroking rate and so this component
536 can be removed by filtering (Sato et al., 2003). To design this filter, we calculated power spectra
537 (FFT length 512, 50% overlap, 25 Hz sampling rate) of the longitudinal and dorso-ventral
538 accelerometer signals during descents and ascents to determine the dominant stroke frequency

539 *sensu* Sato et al. (2007), f_r, for each animal. A symmetric Finite Impulse Response (FIR) low-
540 pass filter, L, was then designed with a cut-off frequency of $0.4f_r$ to separate stroking and
541 postural signals. This filter was applied to each axis of the accelerometer and the filtered data
542 were shortened by removing samples equivalent to half the filter length from the start of each
543 signal, effectively cancelling the group delay of the filter (Stein, 2000). The measured and low-
544 pass filtered accelerometer signals at time, t, are referred to as A_t and $\overline{A}_t$, respectively, with each
545 being a 3-element vector with axes, x (longitudinal), y (lateral) and z (dorso-ventral).
546 The U-shaped deep dives of beaked whales (Baird et al., 2008) naturally divide into three
547 phases: descent, bottom and ascent. To distinguish dive phases, the pitch angle was computed
548 from the low-pass filtered acceleration using $\text{pitch} = \text{asin}(\bar{a}_x/||A_t||)$ with negative pitch angles
549 indicating descent. Following Miller et al. (2004), we defined descents as the interval from the
550 start of the dive until the pitch first exceeds 0º. Ascents are taken as beginning at the last time in
551 the dive with a sustained downward pitch (<0º). The reliability of this method was checked
552 visually and corrected in several cases in which a brief descent occurred in the middle of the
553 ascent or vice versa. Rapid manoeuvring during foraging in the bottom phase makes it difficult to
554 detect individual fluke-strokes and so movements were not analysed in this phase.
555 DTags do not have a speed sensor but assuming that animals move in a caudo–rostral
556 direction, forward speed, $u(t)$, can be estimated by dividing vertical speed (i.e., the differential
557 of depth) by the sine of the instantaneous pitch angle (i.e., $\text{asin}(a_x/||A_t||)$ (Miller et al., 2004).
558 The resulting speed estimate is noisy because of specific acceleration corrupting the pitch
559 estimate and because of noise in the depth sensor amplified by the differentiation, and so requires
560 low-pass filtering. As we are interested in the speed increment over individual fluke strokes, we
561 computed the speed estimate at 25Hz and then low-pass filtered this with a 0.6 Hz cut-off
562 frequency. To minimise errors, this speed estimate was only used when the average absolute
563 pitch angle was more than 30 degrees (Simon et al., 2012). Data analyses were performed in
564 Matlab 7.0 (MathWorks, Natick, USA) and statistical tests were made in R (R Development
565 Core Team, 2009).
566
567 **Rotation and specific acceleration**

Two methods were used to detect and quantify fluke-strokes, leveraging the different sensor suites in the Little Leonardo and DTag tags. The first method requires high sampling rate (i.e., >> twice the stroking rate) accelerometer data which was recorded by both tags. In this method, stroking rate variations were derived by subtracting the low-pass filtered acceleration from the measured acceleration (Sato et al., 2004). The resulting high-pass filtered acceleration, $\widetilde{A}_t = A_t - \overline{A}_t$, contains both rotation and specific acceleration and so cannot be used to quantify either of these movements but it does provide an overall estimate of the magnitude of accelerative signals during stroking. We used the dorso-ventral component of $\widetilde{A}_t$, i.e.,$\tilde{a}_{zt}$ as a proxy for stroking motions that could be computed for all tags.

The second method requires synchronous accelerometer and magnetometer data at high sampling rates so could only be applied to DTag recordings. Magnetometers are sensitive to the instantaneous orientation of the animal but not to its acceleration, providing an opportunity to separate rotation and specific acceleration. As only two orientation angles can be deduced from this triaxial vector sensor, the magnetometer enables precise tracking of body rotations in planar movements independent of acceleration (Bonnet and Héliot, 2007). Here we use this method to track orientation during stroking. In this method (see Appendix section A1), estimated body rotations ($\hat{r}_t$), derived from the high pass filtered magnetometer signals ($\widetilde{M}_t$), are used to predict the dynamic orientation component in the high pass filtered accelerometer signals and so arrive at an estimate of the specific acceleration ($\hat{S}_t$).

Stroking and glide detection

The accelerometer and magnetometer methods described above provide scalar signals, high-pass filtered dorso-ventral acceleration ($\tilde{a}_{zt}$) and estimated body rotations ($\hat{r}_t$), respectively, which can be used to detect intervals with and without stroking. An exploratory examination of these signals suggested that asymmetric and incomplete strokes were common, leading us to analyse stroking on the basis of half strokes. These are defined as the interval between successive zero-crossings in the estimated body rotations, $\hat{r}_t$ for Zc and Md, and $\tilde{a}_{zt}$ for Ha. We used log-frequency plots (Sibly et al., 1990) of these signals to pick suitable hysteretic thresholds, J, for detecting zero-crossings. Stroking was considered to occur whenever there were zero crossings in which the signal passed from below –J to above +J or vice versa within $2/f_r$ seconds, where f_r

is the dominant stroking rate for each animal. Up-strokes were defined as the period between a positive and a negative zero-crossing and down-strokes from negative to a positive zero-crossing. Intervals $> 2/f_r$ between zero crossings were defined as glides. The accuracy of this stroke and glide detection method was checked visually relying on the usually evident differences in stroking and gliding in accelerometer signals. The automatic method was accurate with the exception that partial fluke strokes at the start and end of fluking bouts were often not detected, neither as strokes nor glides, on account of having only one valid zero-crossing. These movements appear to generate little acceleration and may primarily serve to position the flukes for the next gait. Thus, the exclusion of these transitional movements from the analysis has little impact on the results. The lack of a concluding stroke in some dives impedes the method to detect the terminal glide in ascents and these glides were added manually.

Stroke parameters were only calculated for half strokes of Md and Zc in which the single plane rotation model explained more than 80% of the variance in the magnetometer signal (see Appendix section A2). For these half strokes, the duration and root mean square (RMS) magnitude of the stroking signal were calculated along with the RMS of the estimated heave and surge accelerations.

To provide a simple comparison of swimming effort during descents and ascents, and therefore help predict whether whales are denser or less dense than water, the total number of half strokes between 100 and 400 m in each phase was calculated. This depth range excludes depths near the surface in which air in the lungs will contribute more strongly to buoyancy and includes all but 4 deep dives of Md for which the descent phase does not reach the 400 m.

List of symbols, terms and abbreviations

$\mathbf{A_t}$	measured triaxial accelerometer signal in m/s^2 at time t. Components are a_{xt}, a_{yt} and a_{zt}.
$\bar{\mathbf{A}}_\mathbf{t}$	low-pass filtered accelerometer signal in m/s^2 at time t. Components are $\bar{a}_{xt}$, $\bar{a}_{yt}$ and $\bar{a}_{zt}$.
$\tilde{\mathbf{A}}_\mathbf{t}$	high-pass filtered accelerometer signal in m/s^2 at time t. Components are $\tilde{a}_{xt}$, $\tilde{a}_{yt}$ and $\tilde{a}_{zt}$.
B	Local magnetic field vector in the navigation frame. Units are micro-Telsa (μT).
d	peak dorso-ventral displacement of the body in meters during stroking.
$\mathbf{f_r}$	dominant stroke frequency in Hz.
G	Earth's gravity vector in the navigation frame. Units are m/s^2

Ha *Hyperoodon ampullatus.*

J threshold for detecting fluke-strokes.

L symmetric finite impulse response (FIR) low-pass filter.

Md *Mesoplodon densirostris.*

$\mathbf{M_t}$ measured triaxial magnetometer signal in μT. Components are $m_{xt,}$ m_{yt}, m_{zt}

$\bar{\mathbf{M}}_\mathbf{t}$ low-pass filtered magnetometer signal in μT at time t. Components are $\bar{m}_{xt}$, $\bar{m}_{yt}$ and $\bar{m}_{zt}$.

$\tilde{\mathbf{M}}_\mathbf{t}$ high-pass filtered magnetometer signal in μT at time t. Components are $\tilde{m}_{xt}$, $\tilde{m}_{yt}$ and $\tilde{m}_{zt}$.

pitch rotation around the animal's lateral (y) axis.

$\mathbf{Q_t}$ rotation matrix describing the instantaneous orientation of the animal with respect to the navigation frame at time t.

$\bar{\mathbf{Q}}_\mathbf{t}$ rotation matrix describing slowly-varying postural changes.

roll rotation around the animal's longitudinal (x) axis.

$\mathbf{r_t}$ instantaneous pitch angle of the body during stroking.

$\hat{\mathbf{r}}_\mathbf{t}$ estimated instantaneous pitch angle.

$\mathbf{R_t}$ rotation matrix due to stroking rotations.

RMS root mean square.

$\mathbf{S_t}$ specific acceleration vector in the animal frame, m/s^2. Components are $s_{xt,}$ s_{yt} and s_{zt}, i.e., the surge, sway and heave accelerations, respectively.

$\hat{\mathbf{S}}_\mathbf{t}$ estimated triaxial specific acceleration in m/s^2 at time t. Components are $\hat{s}_{xt}$, $\hat{s}_{yt}$ and $\hat{s}_{zt}$.

t time t.

thrust propulsive force produced in the direction of travel by the animal during stroking.

u forward speed.

v vertical speed.

x longitudinal axis. Anterior is positive.

y lateral axis. Positive towards the right.

z dorso-ventral axis. Dorsal is positive.

Zc *Ziphius cavirostris.*

662 **APPENDIX:**

663

664 ***A1: Magnetometer method***

665 Neglecting sensor noise and calibration errors, simplified models for the accelerometer
666 and magnetometer signals while swimming are:

667 $$A_t = Q_t G + S_t \quad \text{(Eqn 1)}$$

668 $$M_t = Q_t B \quad \text{(Eqn 2)}$$

669 where $A_t = [a_{xt}, a_{yt}, a_{zt}]^T$ is the measured acceleration in m/s^2; $M_t = [m_{xt}, m_{yt}, m_{zt}]^T$ is the
670 measured magnetic vector in micro-Telsa (μT), and both vectors are corrected for the tag
671 orientation on the animal; G is the Earth's gravity vector in the navigation frame, i.e., north, east,
672 up; B is the local magnetic field vector in the same frame; S_t is the triaxial specific acceleration
673 with respect to the animal's body axes; and Q_t is a rotation matrix describing the instantaneous
674 orientation of the animal with respect to the navigation frame at time t (Johnson and Tyack
675 2003). The orientation can be factored into two components, $Q_t = R_t\ \bar{Q}_t$ where $\bar{Q}_t$ represents the
676 slowly-varying postural changes and R_t represents higher-rate body rotations due to stroking, i.e.:

677 $$A_t = R_t \bar{Q}_t G + S_t \quad \text{(Eqn 3)}$$

678 $$M_t = R_t \bar{Q}_t B \quad \text{(Eqn 4)}$$

679 In routine swimming, changes in orientation due to manoeuvres generally occur more slowly
680 than do body rotations due to stroking and so these components can be separated by filtering the
681 magnetometer signals. Thus, assuming that R_t has negligible signal below the stroking rate, $\bar{Q}_t B$
682 can be derived from M_t by filtering each axis, i.e., $\bar{M}_t = L\{M_t\} \approx \bar{Q}_t B$ where L is a low pass
683 filter. Here we use a symmetric Finite Impulse Response (FIR) low-pass filter with a cut-off
684 frequency of 0.4 times the dominant stroke frequency (f_r) as defined earlier to separate stroking
685 and postural signals in the accelerometer method. Body rotation in caudal propulsion largely
686 occurs around a single axis (i.e., the y or lateral axis for a cetacean and the x or longitudinal axis
687 for a pinniped). Thus, assuming that the body rotation in cetacean stroking can be approximated
688 by a small-angle pitching rotation with time-varying angle r_t, then
689 $R_t \approx [1 \quad 0 \quad \sin(r_t); 0 \quad 1 \quad 0; -\sin(r_t) \quad 0 \quad 1]$. Applying this simplification to Eqn 4, we
690 obtain:

691 $$M_t \approx \bar{M}_t + \sin(r_t)[\bar{m}_{zt} \quad 0 \quad -\bar{m}_{xt}]^T \quad \text{(Eqn 5)}$$

Hence the difference between the measured and low-pass filtered magnetic vectors is approximately:

$$\tilde{M}_t \triangleq M_t - \bar{M}_t \approx \sin(r_t)[\bar{m}_{zt} \quad 0 \quad -\bar{m}_{xt}]^T \qquad \text{(Eqn 6)}$$

Thus, body rotations during stroking generate signals in both the x and z axes of $\tilde{M}_t$ with the amount in each axis depending on the animal's orientation. A least-squared-error estimator (Demmel, 1997) for body rotations, $\sin(r_t)$, is obtained by pre-multiplying $\tilde{M}_t$ by the vector $W_t = [\bar{m}_{zt} \quad 0 \quad -\bar{m}_{xt}]/(\bar{m}_{zt}^2 + \bar{m}_{xt}^2)$, i.e., the pseudoinverse of the vector on the right hand side of Eqn 6, to get:

$$\hat{r}_t = \mathrm{asin}(W_t \tilde{M}_t) \qquad \text{(Eqn 7)}$$

Where $\hat{r}_t$ is the estimated instantaneous pitch angle of the body rotation during stroking, independent of orientation and specific acceleration. This method, as with any vector field sensor, has the limitation that rotations about an axis parallel to the field vector are unobservable. Thus, stroking will be unobservable in the magnetometer when the animal's lateral axis is parallel with the earth's magnetic field. For Md and Zc tagged in the Canary Islands and the Ligurian Sea, respectively, the magnetic field vector has a downwards inclination of some 45-55°, meaning that postures with a roll angle of > 45° are required for this problem to arise. Rolls of this magnitude are rare during descent and ascent swimming. However, postures in which stroking is unobservable can be readily detected as these give a denominator of zero in W_t. More generally, stroking rotations will have a poor signal-to-noise ratio if $\bar{m}_{zt}^2 + \bar{m}_{xt}^2$ is small compared with $\bar{m}_{yt}^2$. To avoid these potentially noisy data points, we removed orientations for which $(\bar{m}_{zt}^2 + \bar{m}_{xt}^2) < \bar{m}_{yt}^2((1/\cos(25^\circ)^2) - 1)$ from stroking analysis; i.e. when the animal's lateral axis is within 25° of the earth's magnetic field vector. This resulted in removal of 3% of the data points for Md and Zc. Having estimated the body rotation due to stroking, this motion can be removed from the accelerometer signal to leave an estimate of the specific acceleration. To do this, we assume that there is negligible specific acceleration at frequencies below the stroking rate so that low-pass filtering the accelerometer removes both the specific acceleration and body rotation, i.e., $\bar{A}_t = L\{A_t\} \approx \bar{Q}_t G$. Substituting this and the approximation for R_t into Eqn 3 gives:

$$A_t \approx R_t \bar{A}_t + S_t \approx \bar{A}_t + \sin(r_t)[\bar{a}_{zt} \quad 0 \quad -\bar{a}_{xt}]^T + S_t \qquad \text{(Eqn 8)}$$

Thus, the specific acceleration can be estimated from:

$$\hat{S}_t \triangleq [\hat{s}_{xt} \quad \hat{s}_{yt} \quad \hat{s}_{zt}] = \tilde{A}_t - \sin(\hat{r}_t)[\bar{a}_{zt} \quad 0 \quad -\bar{a}_{xt}]^T \qquad \text{(Eqn 9)}$$

where $\sin(r_t)$ in Eqn 8 has been replaced with its estimate from Eqn 7 to compute $\hat{S}_t$. The components of $\hat{S}_t$ in the longitudinal, lateral, and dorso-ventral axes are termed surge, sway and heave accelerations, respectively.

***A2: Stroke selection*:**

The swimming model used to generate $\hat{r}_t$ assumes that the body rotates around the transverse axis, i.e., a pitch rotation. To assess the quality of fit of this movement model for the magnetometer estimator in Eqn 7, we computed the r^2 statistic, i.e., one minus the relative squared residuals $\left\|\tilde{M}_t - \sin(\hat{r}_t)[\bar{m}_{zt} \quad 0 \quad -\bar{m}_{xt}]^T\right\|^2 / \left\|\tilde{M}_t\right\|^2$, for each half stroke. The model provided an acceptable fit (r^2 >0.8) to the magnetometer data in 86% (Md) and 92% (Zc) of half strokes giving an overall r^2 of 0.93 (Md and Zc) for the analysed half strokes. About 12% of half strokes were rejected due to an r^2<0.8. These likely coincided with transient fast manoeuvres for which the spectral separation assumption breaks down. Although stroking may also involve some rolling or yawing rotations, the high r^2 values suggest that the simple pitch model is a good approximation for ascent and descent swimming in Md and Zc.

The r^2 was also computed for the accelerometer estimator of Eqn 9, ignoring specific acceleration, as $1 - \left\|\tilde{A}_t - \sin(\hat{r}_t)[\bar{a}_{zt} \quad 0 \quad -\bar{a}_{xt}]^T\right\|^2 / \left\|\tilde{A}_t\right\|^2$. This was not done to assess quality of fit but rather to give a sense for how well a rotation-only model fits the observed accelerometer signals. The much lower r^2 values of 0.65 (Md and Zc) indicates, as expected, that body rotation explains a smaller part of the accelerometer signals.

A3: Occurrence of B-strokes

To explore the possibility that B-strokes were associated with longer, faster or more vertical swimming we used a generalized linear model (GLM) with a logit link function and two explanatory variables: time into the dive (min) and vertical speed (m/s); as pitch and vertical speed are highly correlated, pitch angle (°) was not included in the model. A mixed effect model was used for Md and Zc with individual as a random effect while a fixed effect model was used

for Ha with individual as a fixed factor due to the small sample size. The presence of one or more B-half-strokes in each 10 s (Md) or 15 s (Zc and Ha) interval in the ascent was used as a dichotomous response variable. These analysis intervals were chosen to encompass the typical stroke-and-glide gait duration for each species. Models were fit using the *lmer* and *glm* functions in R and goodness of fit assessed following Nakagawa and Schielzeth (2013).

Ascent models showed significant positive relationships between occurrence of B-strokes and both vertical speed (odds increase by 17, 13 and 31% for Md, Zc and Ha per meter) and time into dive per interval (odds increase by 11, 13, and 20% for Md, Zc and Ha respectively, per minute). However, these models explain relatively little variance with marginal r^2 (i.e., the variance fraction explained by the fixed effects) of 0.22 (Md), 0.37 (Zc) and 0.50 (Ha). For Md and Zc, the random effect increased the conditional r^2 to 0.45 and 0.51, respectively, indicating considerable individual variability. The weak association of B-strokes with vertical speed may be a consequence of the frequent co-occurrence of B-strokes with glides within the 10 s or 15 s analysis windows. Despite there being 1.2 to 13 times more normal strokes than B-strokes, a high percentage of ascent glides were performed after a B-stroke (85% in Md, 63% in Zc and 67% in Ha). These glides had about 2 to 3.5 times the duration of a normal stroke and so substantially reduced the overall acceleration of the stroke-and-glide gait. To quantify this, we calculated a relative measure of activity, similar to the Vectorial Dynamic Body Acceleration (VeDBA, Gleiss et al., 2011a) during the same ascent intervals. This measure was calculated as the sum of the vector magnitude of $\widetilde{A}_t$ for Ha, and $\hat{S}_t$, for Md and Zc. Intervals with B-strokes had values of this metric that were 1.1-1.5 times greater than intervals with normal stroking (Table 2) with the exception of two Zc for which the B-stroke value was twice the usual stroke value due to occasional bursts of up to 10-14 consecutive B-strokes.

Based on the significant relationship between B-strokes and the elapsed time in a dive, we evaluated when B-strokes began to be produced in dives. The onset time of B-strokes was calculated as the elapsed time from the beginning of each deep dive until the first minute with at least the median rate of B-strokes for each whale. The onset times and the corresponding depths were averaged for each whale, and then pooling animals for species. Although no B-strokes were found in descents, the bottom phase of dives could not be analysed and so these onset times will be biased if B-strokes were used in some dives before the start of the ascent. It is in fact difficult

to assess how these onset times compare to those that would be obtained by chance if B-strokes occurred at random in ascents because of two forms of censoring: left-censoring occurs when B-strokes are found immediately at the start of an ascent whereas right-censoring occurs when no type-B strokes are performed in an ascent. A non-parametric maximum likelihood estimator (NPMLE) allowing interval-censored data was used to estimate type-B stroke onset time for *Mesoplodon* and *Ziphius* (see Supplementary Material, Fig. 1), but not for *Hyperoodon* due to the small sample size. The analysis was carried out in R using the *surv* and *survfit* functions in R package *survival* (Therneau, 2012). Taking into account the interval censored data, B-strokes appeared significantly later than expected by chance (i.e., the raw data confidence intervals for onset time were to the right of the randomized curve). For Md and Zc, B-strokes appeared more than 4 and 6 minutes later than expected by chance, respectively, in 50% of dives.

ACKNOWLEDGEMENTS

We thank A. Crespo, A. Fais, A. Schiavi, A. Escánez, C. Reyes, J. Marrero, K. Gikopoulou, M. Bayona,, M. Moral, M. Tobeña, P. Arranz, P. Madsen, A. Bocconcelli, A. Sturlese, G. Mojoli, M. Ballardini, T. Pusser, K. Aoki, M. Bivins, R. Antunes, T. Narazaki, V. Deecke, and many others for their help in the field in the Canary Islands, Ligurian Sea and The Gully. Special thanks to Mick Wu and Iosu Paradinas Aranjuelo for his statistical support. Thanks also to Mike Fedak, Frants Jensen, Peter T. Madsen, Rene Swift, Ann Pabst, Brandy P. Velten, Peter L. Tyack, Hans M. Nielsen, Paul Ponganis, Gerald Kooyman and the anonymous reviewers for insightful comments which have greatly improved the paper. This paper is dedicated to Guido Mojoli whose enthusiasm kept us going.

COMPETING INTERESTS

The authors have declared that no competing interests exist.

AUTHOR CONTRIBUTIONS

Conceived and designed the experiments: LMML NAS PJOM and MJ. Performed the experiments: LMML NAS PJOM and MJ. Analyzed the data and designed the magnetometer method: LMML and MJ. Wrote the paper: LMML NA PJOM and MJ.

FUNDING

Work in the Canary Islands was funded by the Office of Naval Research and the National Ocean Partnership Program (US), by a consortium consisting of the Canary Islands Government, the Spanish Ministry of Environment and the Spanish Ministry of Defense, and by the European environmental funding LIFE-INDEMARES program for the inventory and designation of the Natura 2000 network in marine areas of the Spanish territory, headed by Fundacion Biodiversidad, with additional support from the Cabildo Insular of El Hierro. Fieldwork in the Ligurian Sea was funded by the National Oceanic Partnership Program (NOPP). Research in the Gully was funded by the Strategic Environmental Research and Development Program (SERDP) programs RC-2113 and RC-2337.

LMML was funded by a 'la Caixa' Fellowship within the 2010 UK Framework Programme. NAS was funded for this study by ONR and by the EU FP7 Marie Curie project SOUNDMAR. MJ was funded by a Marie Curie Career Integration Grant, and from the MASTS pooling initiative (The Marine Alliance for Science and Technology for Scotland) and their support is gratefully acknowledged. MASTS is funded by the Scottish Funding Council (grant reference HR09011) and contributing institutions.

TABLES

Table 1. ***Deep dive statistics during descents and ascents of all tagged individuals.***

Species		Md (n=10)	Zc (n=9)	Ha (n=2)
Dives analysed		49	43	6
Dive duration (mean +/- sd), minutes		49±5	59±12	49±4
Dive depth (mean +/- sd), meters		844±87	1044±199	1572±102
Forward speed (mean, +/- sd), ms^{-1}	Descent	1.5±0.24	1.3±0.06	1.6±0.09
	Ascent	1.2±0.20	1.3±0.10	1.2±0.01

Vertical speed (mean, +/- sd) ms^{-1}	**Descent**	**1.5±0.14****	**1.4±0.12****	**1.8±0.04****
	Ascent	**0.7±0.10****	**0.8±0.15****	**1.3±0.03****
Pitch angle (mean, +/- sd), degrees	**Descent**	**61±5****	**65±7****	**63±9**
	Ascent	**33±6****	**38±11****	**63±1**
Distance covered (100-400m), (mean, +/- sd), m	Descent	333±25	324±18	314±4
	Ascent	586±102	470±71	370±9
Total glide duration (100-400m), (mean, +/- sd) min	**Descent**	**2.1±0.7****	**2.6±0.7****	**1.8±0.1***
	Ascent	**1.0±0.4****	**0.9±0.5****	**0.7±0.4***
Total half-strokes (100-400m), (mean, +/- sd)	Descent	68±50	92±18	32±5
	Ascent	172±28	80±18	64±9
% type-B half-strokes (100-400) , (mean, +/- sd)	Descent	5±5	3±5	9±11
	Ascent	34±15	47±22	32±10
Normal-stroke frequency (mean, +/- sd), Hz		0.44±0.06	0.36±0.03	0.32±0.00
B-stroke frequency (mean, +/- sd), Hz		0.58±0.07	0.48±0.06	0.45±0.05

n=number of tag deployments for each species

'mean' is the mean of individual means of the parameter.

'sd' is the standard deviation of individual means

Pairs of each dive ascent/descent parameters tested with a *paired t-test* are shown in bold. Forward speed and distance covered were computed from vertical speed and pitch and so were not separately tested.

Percentage of total half-strokes and type-B strokes were not tested because the difference in descent vs. ascent is evident.

** indicates a highly significant difference ($p<0.001$) between descent and ascent parameters

* means a significant difference ($p<0.05$)

No symbol means no significant difference ($p>0.05$)

837

Table 2. ***Comparison of the parameters and occurrence of normal and B-strokes within the ascents Asc and descents Desc of all tagged individuals.*** *Acc and Mag refer to the two analysis methods developed here: the Acc,* $\tilde{a}_{zt}$*, method uses only the accelerometer while the Mag,* $\hat{r}_t$*,method derives body rotation from the magnetometer and then estimates heave and surge accelerations from the accelerometer.*

Tag ID	Dive phase	Magnitude Ratio B/ Normal $\tilde{a}_{zt}$	Magnitude Ratio B/ Normal $\hat{r}_t$	Threshold $\hat{s}_{zt}$ or $\tilde{a}_{zt}$ B/Normal	Duration ratio B/ Normal	Surge ratio B/Normal	Heave ratio B/Normal	VeDBA Gait Ratio cont/s&g
Md03_284a/MdH1-03	Asc	2.18	1.32	0.50	0.77	4.02	2.72	1.14
Md08_137a/MdH1-08	Asc	3.27	1.58	0.65	0.78	3.99	3.46	1.10
Md03_298a/MdH15-03	Asc	2.61	1.59	0.65	0.82	4.20	3.00	1.41
Md04_287a/MdH22-04	Asc	2.66	1.70	0.80	0.82	3.73	2.84	1.34
Md08_289a/MdH22-08	Asc	3.48	1.47	0.65	0.77	4.35	3.55	1.31
Md05_277a/MdH6-05	Asc	2.21	1.36	0.50	0.77	2.99	3.14	1.15
Md08_136a/MdH6-08	Asc	2.18	1.35	0.46	0.75	4.29	2.58	1.18
Md05_285a/MdH43-05	Asc	2.18	1.33	0.80	0.66	3.64	3.77	1.36
Md08_148a/MdHC1-08	Asc	2.55	1.53	0.80	0.76	4.30	3.40	1.23
Md10_163a/MdH86-10	Asc	2.33	1.45	0.70	0.80	3.73	2.55	1.18
Md mean ± sd	**Asc**	**2.52±0.53**	**1.47±0.13**		**0.77±0.04**	**3.92±0.42**	**3.10±0.43**	**1.24±0.11**
Md mean ± sd	**Desc**	**1.54±0.16**	**1.35±0.15**		**0.86±0.08**	**1.99±0.25**	**2.17±0.26**	
Zc04_160a	Asc	2.56	1.69	0.85	0.71	4.16	3.26	1.28
Zc04_161a	Asc	4.75	1.86	2.50*	0.62	5.76	5.29	1.31
Zc04_161b	Asc	2.22	1.68	1.30*	0.70	3.83	3.59	2.74
Zc04_175a	Asc	2.06	1.46	0.35*	0.82	3.34	2.92	1.81
Zc04_179a	Asc	2.79	1.61	0.40	0.77	3.69	3.45	1.17
Zc05_167a	Asc	2.13	1.50	0.40*	0.79	3.47	3.11	1.25
Zc05_170a	Asc	2.03	1.49	2.00	0.78	3.81	3.22	1.16
Zc06_205a	Asc	2.70	1.41	0.80*	0.75	4.23	3.43	1.23
Zc mean ± sd	**Asc**	**2.60±0.85**	**1.58±0.15**		**0.75±0.07**	**3.98±0.73**	**3.46±0.72**	**1.49±0.51**
Zc mean ± sd	**Desc**	**1.65±0.19**	**1.32±0.12**		**0.74±0.07**	**2.52±0.62**	**2.65±0.51**	
Ha11_219a	Asc	2.56		1.20	0.67	2.64	2.56	1.09
Ha11_223a	Asc	2.28		1.40	0.71	1.83	2.28	1.04
Ha mean ± sd	**Asc**	**2.42±0.20**			**0.69±0.03**	**2.24±0.57**	**2.42±0.20**	**1.07±0.03**
Ha mean ± sd	**Desc**	**2.28±0.16**			**0.70±0.09**	**1.74±1.15**	**2.28±0.16**	

Tag ID: For Md, Zc and Ha the code comprises the species initials, the year (two digits), the Julian day, and the tag deployment of the day (a single letter). In addition for Md the second code (in grey) refers to individuals in the photo-ID catalogue at http://www.cetabase.info, followed by the year (two digits) of the deployment. Shaded cells correspond to data analysed under the Acc method which only uses accelerometer, such as for Ha whose data lacks a high sampling rate magnetometer, while the Mag method is used to obtain the rest of the results. B: Type-B strokes; Normal: normal strokes; VeDBA: Vectorial Dynamic Body Acceleration; cont: continuous stroking gait; s&g: stroke-and-glide gait; Strokes with a signal $\hat{s}_{zt}$ or $\tilde{a}_{zt}$ > threshold are defined as B-strokes. Values for mean refer to mean ± standard deviation. * indicates the average of thresholds across dives within the same animal as the tag had moved during the deployment. For the analysis a different threshold was used for the required dives.

838

FIGURE CAPTIONS

Figure 1. Tag data recorded during a *Mesoplodon densirostris* deep foraging dive (MdH1-03). (A) Depth profile and (B) smoothed pitch angle, of the whale with the descent and ascent phases indicated by blue rectangles. (C-D) High-pass filtered dorso-ventral acceleration, $\tilde{a}_{zt}$, over the descent and ascent intervals with stroking periods coloured black and gliding periods red. The higher-magnitude signals beginning at minute 38 are termed type-B strokes (green arrow), while the smaller amplitude signals are normal strokes.

Figure 2. High-pass filtered Z-axis acceleration ($\tilde{a}_{zt}$) during ascents showing mixed gaits for A: *Mesoplodon,* B: *Ziphius,* C: *Hyperoodon.* Each panel illustrates the first occurrence of type-B strokes (green arrow) in the ascent phase.

Figure 3. Detailed view of the high pass filtered z-axis accelerometer ($\tilde{a}_{zt}$, panel A) and estimated body rotation ($\hat{r}_t$, panel B) signals during an ascent of MdH1-03 showing the typical mixed gait. The dashed line represents the threshold (+/-J) used to detect zero-crossings and to distinguish gliding intervals (see Material and Methods stroking and glide detection section). Half strokes are coloured blue for normal and green for B-strokes based on the magnitude of the estimated heave signal (see text). Uncoloured periods are transition periods between glides and stroking which were not analysed. B-strokes are evident in the accelerometer which is sensitive to both rotation and specific acceleration but are less apparent in the rotation signal which is derived from the magnetometer and so is insensitive to specific acceleration.

Figure 4. Scatter plots of half fluke-stroke (n= 2996) duration (taken from zero-crossings in the body rotation signal derived from the magnetometer) versus rotation angle and three acceleration measures. The plots cover 5 deep dive ascents by a *Mesoplodon densirostris,*

MdH1-03. In each panel up-strokes are coloured brighter while down-strokes are coloured in darker; the resulting clusters are coloured in green (B-strokes) and blue (normal strokes). (A) RMS of the body rotation, $\hat{r}_t$. (B) RMS of the dorso-ventral acceleration, $\tilde{a}_{zt}$. (C-D) RMS of the surge $\hat{s}_{xt}$ and heave acceleration, $\hat{s}_{zt}$, as predicted from the magnetometer and accelerometer. For this animal, a heave acceleration threshold of 0.5 ms^{-2} can be used to separate clusters and so differentiate type-B half-strokes (i.e., RMS heave >0.5 ms^{-2};colored in green) from normal half-strokes (coloured in blue). Similar patterns were observed for Zc and Ha whales. For Ha, the heave could not be estimated due to low magnetometer sampling rate and so strokes were differentiated by a threshold in the RMS $\tilde{a}_{zt}$.

Figure 5. Estimated body rotations $\hat{r}_t$ (A), and forward speed u (B) compared to surge $\hat{s}_{xt}$ (C) and heave $\hat{s}_{zt}$ (D) accelerations during a *Ziphius* (Zc05_167a) steep (>40 degrees) ascent period. Speed was calculated from the vertical speed divided by the sin(pitch) sampled at 25 Hz, and was then smoothed with a low pass filter of 0.6Hz. Gliding periods, normal and B strokes are coloured red, blue and green respectively. The timing of strokes is taken from the rotation signal,$\hat{r}_t$.

Figure 6. Detailed view of ascent fluking by a *Mesoplodon* (MdH1-03) showing the typical mixed gait comprising normal half-strokes (blue), B-half-strokes (green) and glides (red). (A) Body rotation $\hat{r}_t$. Dashed line represents the threshold (+/-J) used to detect zero-crossings and to distinguish gliding intervals. (B) High frequency dorso-ventral acceleration, $\tilde{a}_{zt}$. (C) and (D): estimated surge and heave acceleration $\hat{s}_{xt}$ and $\hat{s}_{zt}$, respectively in m/s^2. Glides are shown in red. Uncoloured periods are transition periods between glides and stroking which were not analysed. At this tag location (approximately midway between blow-hole and dorsal fin), surge and heave acceleration are some 90 degrees out of phase with body rotation with positive surge peaks occurring as the body at the tag position rotates through zero in a downwards direction. B-strokes sometimes appear as a single half-stroke (e.g., second 5) with just one large peak in surge and heave acceleration but others as a full stroke (e.g., second 24).

REFERENCES

Aguilar de Soto, N., Johnson, M. P., Madsen, P. T., Díaz, F., Domínguez, I., Brito, A. and Tyack, P. L. (2008). Cheetahs of the deep sea: deep foraging sprints in short-finned pilot whales off Tenerife (Canary Islands). *J. Anim. Ecol.* **77**, 936–947.

Aguilar de Soto, N., Madsen, P. T., Tyack, P. L., Arranz, P., Marrero, J., Fais, A., Revelli, E. and Johnson, M. P. (2012). No shallow talk: Cryptic strategy in the vocal communication of Blainville's beaked whales. *Mar. Mam. Sci.* **28**, 75–92.

Alexander, R McN. (2003). *Principles of Animal Locomotion.* Princeton: Princeton University Press.

Alexander, R. McN. and Goldspink, G. (1977). *Mechanics and Energetics of Animal Locomotion*. London: Chapman and Hall.

Allen, S. G., Mortenson, J. and Webb, S. (2011a). Blainville's beaked whale (*Mesoplodon densirostris*). In, *Field Guide to Marine Mammals of the Pacific Coast: Baja, California, Oregon, Washington, British Columbia,* pp. 223–229. Berkeley: University of California Press.

Allen, S. G., Mortenson, J. and Webb, S. (2011b). Cuvier's beaked whale (Ziphius cavirostris). In, *Field Guide to Marine Mammals of the Pacific Coast: Baja, California, Oregon, Washington, British Columbia,* pp. 215–222. Berkeley: University of California Press.

Aoki, K., Amano, M., Mori, K., Kourogi, A., Kubodera, T. and Miyazaki, N. (2012). Active hunting by deep-diving sperm whales: 3D dive profiles and maneuvers during bursts of speed. *Mar. Ecol. Prog. Ser.* **444**, 289–301.

Arranz, P., Aguilar de Soto, N., Madsen, P. T., Brito, A., Bordes, F. and Johnson, M. P. (2011). Following a foraging fish-finder: diel habitat use of Blainville's beaked whales revealed by echolocation. *PLoS ONE*, **6**, e28353.

Baird, R. W., Webster, D. L., McSweeney, D. J., Ligon, A. D., Schorr, G. S. and Barlow, J. (2006). Diving behaviour of Cuvier's (*Ziphius cavirostris*) and Blainville's (*Mesoplodon densirostris*) beaked whales in Hawai ' i. *Can. J. Zool.* **1128**, 1120–1128.

Baird, R. W., Webster, D. L., Schorr, G. S., McSweeney, D. J. and Barlow, J. (2008). Diel variation in beaked whale diving behavior. *Mar. Mam. Sci.* **24**, 630–642.

Biuw, M., McConnell, B., Bradshaw, C. J. A., Burton, H. R. and Fernández, A. (2003). Blubber and buoyancy: monitoring the body condition of free-ranging seals using simple dive characteristics. *J. Exp. Biol.* **206**, 3405–3423.

Blake, R. W. (2004). Fish functional design and swimming performance. *J. Fish. Biol.* **65**, 1193–1222.

Bonnet, S. and Héliot, R. (2007). A magnetometer-based approach for studying human movements. *IEEE Trans. Biomed. Eng.* **54**, 1353–1355.

Butler, P. J. and Jones, D. R. (1997). Physiology of diving of birds and mammals. *Physiol. Rev.* **77**, 837–899.

Cook, T. R., Kato, A., Tanaka, Hideji, Ropert-Coudert, Y. and Bost, Charles-André (2010). Buoyancy under control: underwater locomotor performance in a deep diving seabird suggests respiratory strategies for reducing foraging effort. *PLoS ONE*, **5**, e9839.

Davis, R. W. (2014). A review of the multi-level adaptations for maximizing aerobic dive duration in marine mammals: from biochemistry to behavior. *J. Comp. Physiol. B*, **184**, 23–53.

Davis, R. W., Fuiman, L. A., Williams, T. M. and Le Boeuf, B. J. (2001). Three-dimensional movements and swimming activity of a northern elephant seal. *Comp. Biochem. Physiol. A Mol. Integr.Physiol.* **129**, 759–770.

Demmel, J.W. (1997). *Applied Numerical Linear Algebra*. Chapter 3. Philadelphia: SIAM Press.

Fish, F. E. (2010). Swimming strategies for energy economy. In *Fish Locomotion: An Etho-ecological Perspective* (ed. P. Domenici and B. G. Kapoor), pp. 90–122. Enfield, NH: Science Publishers.

Fish, F. E., Insley, S. J. and Ronald, K. (1988). Kinematics and estimated thrust production of swimming harp and ringed seals. *J. Exp. Biol.* **137**, 157–173.

Fish, F. E., Fegely, J. F. and Xanthopoulos, C. J. (1991). Burst-and-coast swimming in schooling fish (*Notemigonus crysoleucas*) with implications for energy economy. *Comp. Biochem. Physiol.* **100**, 633–637.

Fish, F. E. and Rohr, J. J. (1999). Review of dolphin hydrodynamics and swimming performance. In *SPAWARS System Center Technical Report 1801*. San Diego, CA.

Fish, F. E., Peacock, J. E. and Rohr, J. J. (2003). Stabilization mechanism in swimming odontocete cetaceans by phased movements. *Mar. Mam. Sci.* **19**, 515–528.

Fish, F. E., Legac, P., Williams, T. M., and Wei, T. (2014). Measurement of hydrodynamic force generation by swimming dolphins using bubble DPIV. *J. Exp. Biol.* **217**, 252-260.

Flammang, B. E. and Lauder, G. V (2008). Speed-dependent intrinsic caudal fin muscle recruitment during steady swimming in bluegill sunfish, *Lepomis macrochirus*. *J. Exp. Biol.* **211**, 587–598.

Fossette, S., Gleiss, A. C., Myers, A. E., Garner, S., Liebsch, N., Whitney, N. M., Hays, G. C., Wilson, R. P. and Lutcavage, M. E. (2010). Behaviour and buoyancy regulation in the deepest-diving reptile: the leatherback turtle. *J. Exp. Biol.* **213**, 4074–4083.

Van Ginneken, V., Antonissen, E., Müller, U. K., Booms, R., Eding, E., Verreth, J. and Van den Thillart, G. (2005). Eel migration to the Sargasso: remarkably high swimming efficiency and low energy costs. *J. Exp. Biol.* **208**, 1329–1335.

Gleiss, A. C., Wilson, R. P. and Shepard, E. L. C. (2011a). Making overall dynamic body acceleration work: on the theory of acceleration as a proxy for energy expenditure. *Methods Ecol. Evol.* **2**, 23–33.

Gleiss, A. C., Norman, B. and Wilson, R. P. (2011b). Moved by that sinking feeling: variable diving geometry underlies movement strategies in whale sharks. *Funct. Ecol.* **25**, 595–607.

Halsey, L. G., Butler, P. J. and Blackburn, T. M. (2006). A phylogenetic analysis of the allometry of diving. *Am. Nat.* **167**, 276–287.

Hays, G. C., Marshall, G. J. and Seminoff, J. A. (2007). Flipper beat frequency and amplitude changes in diving green turtles, *Chelonia mydas*. *Mar. Biol.* **150**, 1003–1009.

Hooker, S. K. and Baird, R. W. (1999). Deep-diving behaviour of the northern bottlenose whale, *Hyperoodon ampullatus* (Cetacea: Ziphiidae). *Proc. R. Soc. of Lond. B Biol. Sci.* **266**, 671–676.

Houtman, C. J., Stegeman, D. F., Van Dijk, J. P. and Zwarts, M. J. (2003). Changes in muscle fiber conduction velocity indicate recruitment of distinct motor unit populations. *J. Appl. Physiol. 95*(3), 1045–1054.

Jayne, B. C. and Lauder, G. V. (1994). How swimming fish use slow and fast muscle fibers: implications for models of vertebrate muscle recruitment. *J. Comp. Physiol. A.* **175**, 123–131.

Johnson, M. P. and Tyack, P. L. (2003). A digital acoustic recording tag for measuring the response of wild marine mammals to sound. *J. Ocean. Eng.* **28**, 3–12.

Johnson, T. P., Syme, D. A., Jayne, B. C., Lauder, V. and Bennett, A. F. (1994). Modeling red muscle power output during steady and unsteady swimming in largemouth bass. *Am. J. Physiol.* **267**, 481–488.

Kanatous, S. B., Davis, R. W., Watson, R. R., Polasek, L., Williams, T. M. and Mathieu-Costello, O. (2002). Aerobic capacities in the skeletal muscles of Weddell seals: key to longer dive durations? *J. Exp. Biol.* **205**, 3601–3608.

Kanatous, S. B., Hawke, T. J., Trumble, S. J., Pearson, L. E., Watson, R. R., Garry, D. J., Williams, T. M. and Davis, R. W. (2008). The ontogeny of aerobic and diving capacity in the skeletal muscles of Weddell seals. *J. Exp. Biol.* **211**, 2559–2565.

De Knegt, H. J., Hengeveld, G. M., Van Langevelde, F., De Boer, W. F. and Kirkman, K. P. (2007). Patch density determines movement patterns and foraging efficiency of large herbivores. *Behav. Ecol.* **18**, 1065–1072.

Kooyman, G. L. and Ponganis, P. J. (1998). The physiological basis of diving to depth: birds and mammals. *Annu. Rev. Physiol.* **60**, 19–32.

Kramer, D. L. (1988). The behavioral ecology of air breathing by aquatic animals. *Can. J. Zool.* **66**, 89–94.

Lovvorn, J. R. and Jones (1991). Effects of body size, body fat, and change in pressure with depth on buoyancy and costs of diving in ducks (*Aythya spp.*). *Can. J. Zool.* **69**, 2879–2887.

Madsen, P. T., Johnson, M. P., Aguilar de Soto, N., Zimmer, W. M. X. and Tyack, P. L. (2005). Biosonar performance of foraging beaked whales (*Mesoplodon densirostris*). *J. Exp. Biol.* **208**, 181–194.

Martin, A. R. and Smith, T. G. (1999). Strategy and capability of wild belugas, *Delphinapterus leucas*, during deep, benthic diving. *J. Exp. Zool.* **77**, 1783–1793.

Mead, J. G. (1989). Beaked whales of the genus Mesoplodon. In *Handbook of Marine Mammals* (ed. S. Ridgway and S. Harrison), pp. 349–430. London: Academic Press.

Miller, P. J. O., Johnson, M. P., Tyack, P. L. and Terray, E. A. (2004). Swimming gaits, passive drag and buoyancy of diving sperm whales *Physeter macrocephalus. J. Exp. Biol.* **207**, 1953–1967.

Miller, P. J. O., Biuw, M., Watanabe, Y. Y., Thompson, D. and Fedak, M. A. (2012). Sink fast and swim harder! Round-trip cost-of-transport for buoyant divers. *J. Exp. Biol.* **215**, 3622–3630.

Mori, Y., Takahashi, A., Trathan, P. N. and Watanuki, Y. (2010). Optimal stroke frequency during diving activity in seabirds. *Aquat. Biol.* **8**, 247–257.**Nakagawa, S. and Schielzeth, H.** (2013). A general and simple method for obtaining R 2 from generalized linear mixed-effects models. *Methods Ecol. Evol*. **4**, 133–142.

Nakagawa, S. and Schielzeth, H. (2013). A general and simple method for obtaining R 2 from generalized linear mixed-effects models. *Methods Ecol. Evol.*, **4**, 133–142.

Noda, T, Okuyama, J., Koizumi, T., Arai, N. and Kobayashi, M. (2012). Monitoring attitude and dynamic acceleration of free-moving aquatic animals using a gyroscope. *Aquat. Biol.* **16**, 265–276.

Noren, S. R., Biedenbach, G. and Edwards, E. F. (2006). Ontogeny of swim performance and mechanics in bottlenose dolphins (*Tursiops truncatus*). *J. Exp. Biol.* **209**, 4724–4731.

R Development Core Team (2009). *R: A language and environment for statistical computing.* Vienna: R Foundation for Statistical Computing: www.R-project.org.

Rome, L. C. (1992). Scaling of muscle fibres and locomotion. *J. Exp. Biol.* **168**, 243–252.

Sato, K., Mitani, Y., Cameron, M. F., Sniff, D. B. and Naito, Y. (2003). Factors affecting stroking patterns and body angle in diving Weddell seals under natural conditions. *J. Exp. Biol.* **206**, 1461–1470.

Sato, K., Charrassin, J., Bost, C. A. and Naito, Y. (2004). Why do macaroni penguins choose shallow body angles that result in longer descent and ascent durations? *J. Exp. Biol.* 4057–4065.

Sato, K., Watanuki, Y., Takahashi, A., Miller, P. J. O., Tanaka, H., Kawabe, R., Ponganis, P. J., Handrich, Y., Akamatsu, T., Watanabe, Y. et al. (2007). Stroke frequency, but not swimming speed, is related to body size in free-ranging seabirds, pinnipeds and cetaceans. *Proc. R. Soc. of Lond. B Biol. Sci.* **274**, 471–477.

Sato, K., Aoki, K., Watanabe, Y. Y. and Miller, P. J. O. (2013). Neutral buoyancy is optimal to minimize the cost of transport in horizontally swimming seals. *Sci. Rep.* **3**, 2205

Schorr, G. S., Falcone, E. a., Moretti, D. J. and Andrews, R. D. (2014). First long-term behavioral records from Cuvier's beaked whales (*Ziphius cavirostris*) reveal record-breaking dives. *PLoS ONE*, **9**, e92633.

Sibly, R. M., Nott, H. M. R. and Fletcher, D. J. (1990). Splitting behaviour into bouts. *Anim. Behav.* **39**, 63–69.

Silva, M. and Downing, J. A. (1995). CRC handbook of mammalian body masses. Boca Raton, FL: CRC Press.

Simon, M., Johnson, M. P., Tyack, P. L. and Madsen, P. T. (2009). Behaviour and kinematics of continuous ram filtration in bowhead whales (*Balaena mysticetus*). *Proc. R. Soc. of Lond. B Biol. Sci.***276**, 3819–3828.

Simon, M., Johnson, M. P. and Madsen, P. T. (2012). Keeping momentum with a mouthful of water: behavior and kinematics of humpback whale lunge feeding. *J. Exp. Biol.* **215**, 3786–3798.

Skrovan, R. C., Williams, T. M., Berry, P. S., Moore, P. W. and Davis, R. W. (1999). The diving physiology of Bottlenose dolphins (*Tursiops truncatus*) II. Biomechanics and changes in buoyancy at depth. *J. Exp. Biol.* **202**, 2749–2761.

Stein, J.Y. (2000). *Digital Signal Processing: A Computer Science Perspective.* New York: John Wiley and Sons Press.

Svendsen, J. C., Tudorache, C., Jordan, A. D., Steffensen, J. F., Aarestrup, K. and Domenici, Paolo (2010). Partition of aerobic and anaerobic swimming costs related to gait transitions in a labriform swimmer. *J. Exp. Biol.* **213**, 2177–2183.

Therneau, T. (2012). Survival: *A Package for survival analysis in S*. R package version 2.37-2 http://CRAN.R-project.org/package=survival.

True, F. N. (1910). An account of the beaked whales of the family Ziphiidae in the collection of the United States National Museum, with remarks on some specimens in other American museums. *Bull. U. S. nat. Mus.* **73**, 1-89.

Tyack, P. L., Johnson, M. P., Aguilar de Soto, N., Sturlese, A. and Madsen, P. T. (2006). Extreme diving of beaked whales. *J. Exp. Biol.* **209**, 4238–4253.

Velten, B. P., Dillaman, R. M., Kinsey, S. T., McLellan, W. A. and Pabst, D. A. (2013). Novel locomotor muscle design in extreme deep-diving whales. *J. Exp. Biol.* **216**, 1862–1871.

Watwood, S. L., Miller, P. J. O., Johnson, M. P., Madsen, P. T. and Tyack, P. L. (2006). Deep-diving foraging behaviour of sperm whales (*Physeter macrocephalus*). *J. Anim. Ecol.* **75**, 814–825.

Webb, P. W. (1994a). Exercise performance of fish. In *Advances in Veterinary Science and Comparative Medicine* (ed. J. H. Jones), 38B, pp. 1-49. Academic Press, Orlando.

Webb, P. W. (1994b). The biology of fish swimming. In *Mechanics and Physiology of Animal Swimming* (ed. L. Maddock, Q. Bone, and J. M. V. Rayner), pp. 45-62. Cambridge University Press, Cambridge, UK.

Webber, D. M. and O'Dor, R. K. (1991). Invertebrate athletes: trade-offs between transport efficiency and power density in cephalopod evolution. *J. Exp. Biol.* **112**, 93–112.

Weihs, D. (1974). Energetic advantages of burst swimming of fish. *J. Theor. Biol.* **48**, 215–229.

White, C. R., Blackburn, T. M. and Seymour, R. S. (2009). Phylogenetically informed analysis of the allometry of mammalian basal metabolic rate supports neither geometric nor quarter-power scaling. *Evolution*, **63**, 2658–2667.

Williams, T. M. (1996). Strategies for reducing foraging costs in dolphins. In *Aquatic Predators and their Prey* (ed. S.P.R. Greenstreet and M.L.Tasker), pp. 4–9. Cambridge: Blackwell Scientific Publications, Oxford.

Williams, T. M. (1999). The evolution of cost efficient swimming in marine mammals: limits to energetic optimization. *Phil.Trans. R. Soc. B Biol. Sci.* **354**, 193–201.

Williams, T. M., Davis, R. W., Fuiman, L. A., Francis, J., Le Boeuf, B. J., Calambokidis, J. and Croll, D. A. (2000). Sink or swim: strategies for cost-efficient diving by marine mammals. *Science*, **288**, 133–136.

Williams, T. M., Fuiman, L. A., Horning, M. and Davis, R. W. (2004). The cost of foraging by a marine predator, the Weddell seal *Leptonychotes weddellii*: pricing by the stroke. *J. Exp. Biol.* **207**, 973–982.

Williams, T. M., Noren, S. R. and Glenn, M. (2011). Extreme physiological adaptations as predictors of climate-change sensitivity in the narwhal, *Monodon monoceros*. *Mar. Mam. Sci.* **27**, 334–349.

Wilson, R. P. and Liebsch, N. (2003). Up-beat motion in swinging limbs: new insights into assessing movement in free-living aquatic vertebrates. *Mar. Biol.* **142**, 537–547.

Wilson, R. P., White, C. R., Quintana, F., Halsey, L. G., Liebsch, N., Martin, G. R. and Butler, P. J. (2006). Moving towards acceleration for estimates of activity-specific metabolic rate in free-living animals: the case of the cormorant. *J. Anim. Ecol.* **75**, 1081–1090.

Zimmer, W. M. X., Johnson, M. P., Madsen, P. T. and Tyack, P. L. (2005). Echolocation clicks of free-ranging Cuvier's beaked whales (*Ziphius cavirostris*). *J. Acoust. Soc. Am.* **117**, 3919–3927.

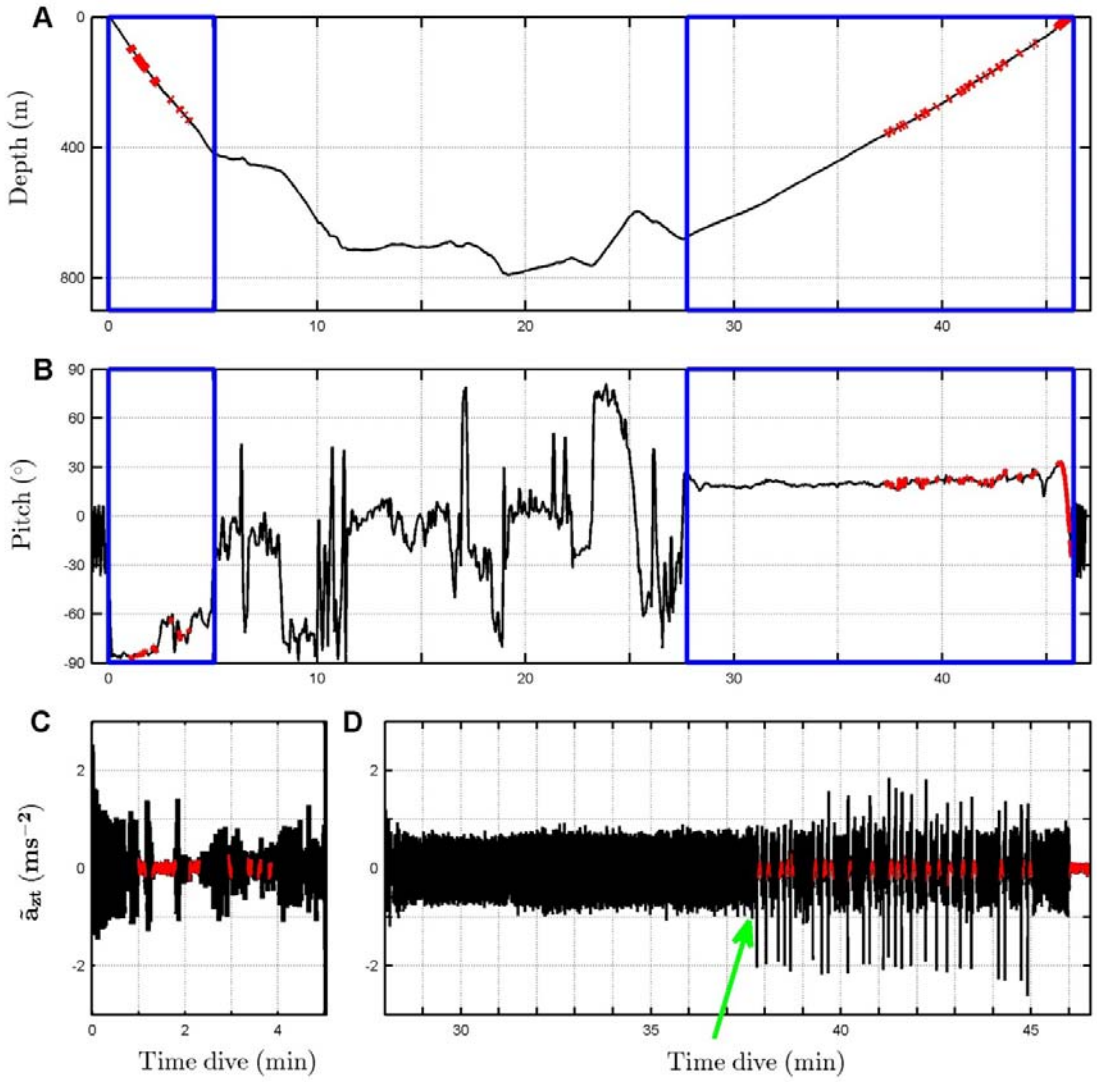

Figure 1. Tag data recorded during a *Mesoplodon densirostris* deep foraging dive (MdH1-03). (A) Depth profile and (B) smoothed pitch angle, of the whale with the descent and ascent phases indicated by blue rectangles. (C-D) High-pass filtered dorso-ventral acceleration, $\tilde{a}_{zt}$, over the descent and ascent intervals with stroking periods coloured black and gliding periods red. The higher-magnitude signals beginning at minute 38 are termed type-B strokes (green arrow), while the smaller amplitude signals are normal strokes.

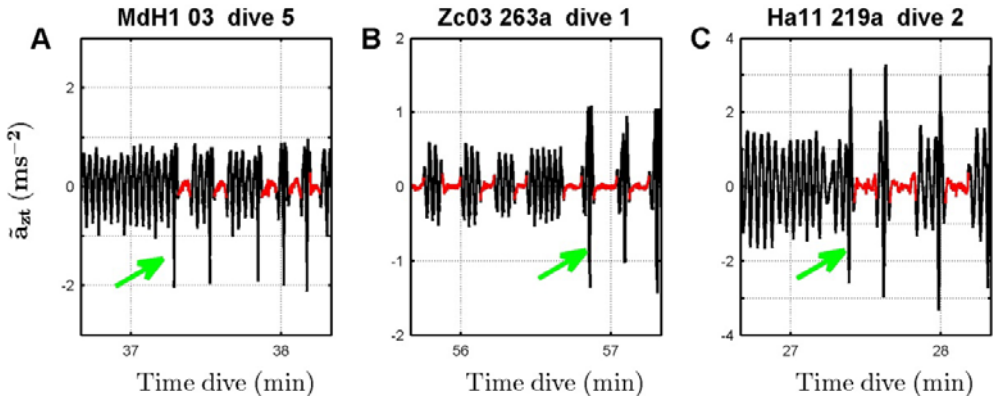

Figure 2. High-pass filtered Z-axis acceleration ($\tilde{a}_{zt}$) during ascents showing mixed gaits for A: *Mesoplodon,* B: *Ziphius,* C: *Hyperoodon.* Each panel illustrates the first occurrence of type-B strokes (green arrow) in the ascent phase.

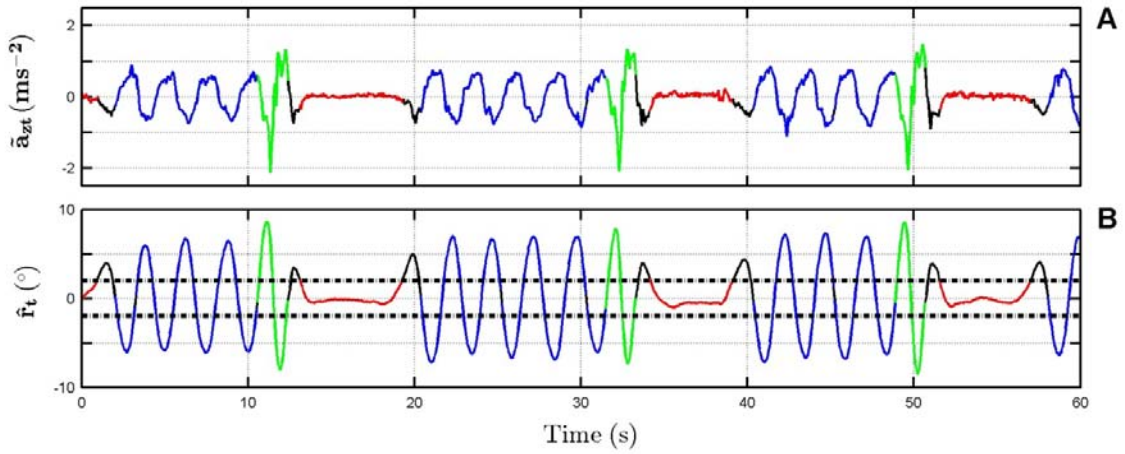

Figure 3. Detailed view of the high pass filtered z-axis accelerometer ($\tilde{a}_{zt}$, panel A) and estimated body rotation ($\hat{r}_t$, panel B) signals during an ascent of MdH1-03 showing the typical mixed gait. The dashed line represents the threshold (+/-J) used to detect zero-crossings and to distinguish gliding intervals (see Material and Methods stroking and glide detection section). Half strokes are coloured blue for normal and green for B-strokes based on the magnitude of the estimated heave signal (see text). Uncoloured periods are transition periods between glides and stroking which were not analysed. B-strokes are evident in the accelerometer which is sensitive to both rotation and specific acceleration but are less apparent in the rotation signal which is derived from the magnetometer and so is insensitive to specific acceleration.

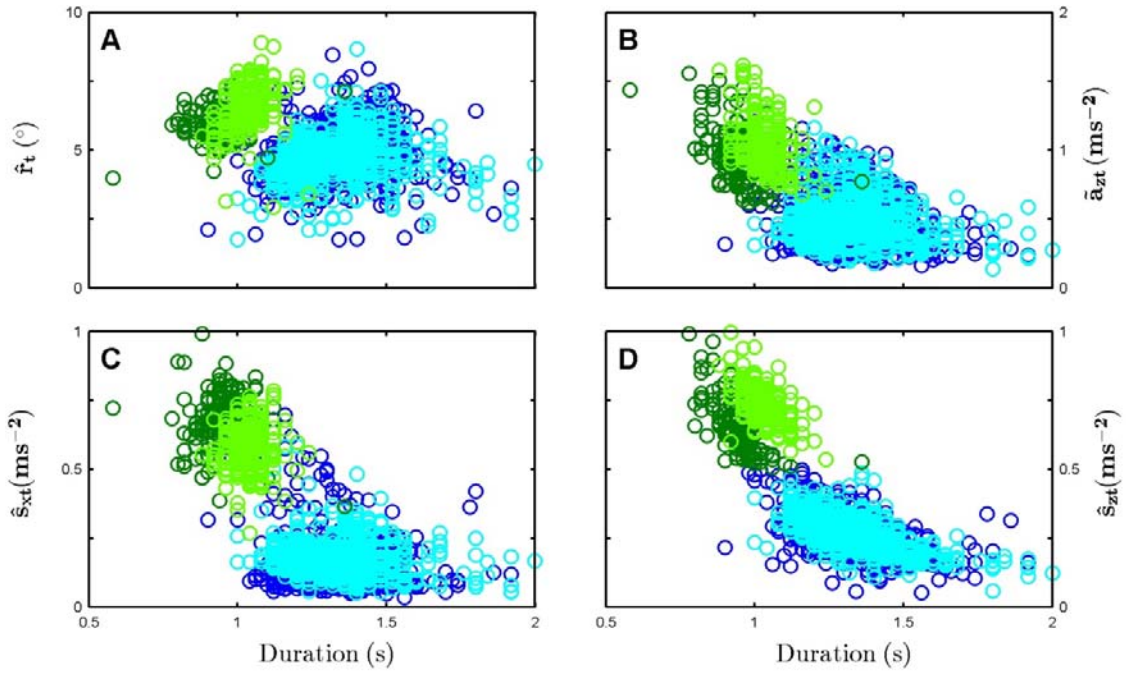

Figure 4. Scatter plots of half fluke-stroke (n= 2996) duration (taken from zero-crossings in the body rotation signal derived from the magnetometer) versus rotation angle and three acceleration measures. The plots cover 5 deep dive ascents by a *Mesoplodon densirostris*, MdH1-03. In each panel up-strokes are coloured brighter while down-strokes are coloured in darker; the resulting clusters are coloured in green (B-strokes) and blue (normal strokes). (A) RMS of the body rotation, $\hat{r}_t$. (B) RMS of the dorso-ventral acceleration, $\tilde{a}_{zt}$. (C-D) RMS of the surge $\hat{s}_{xt}$ and heave acceleration, $\hat{s}_{zt}$, as predicted from the magnetometer and accelerometer. For this animal, a heave acceleration threshold of 0.5 ms^{-2} can be used to separate clusters and so differentiate type-B half-strokes (i.e., RMS heave >0.5 ms^{-2};colored in green) from normal half-strokes (coloured in blue). Similar patterns were observed for Zc and Ha whales. For Ha, the heave could not be estimated due to low magnetometer sampling rate and so strokes were differentiated by a threshold in the RMS $\tilde{a}_{zt}$.

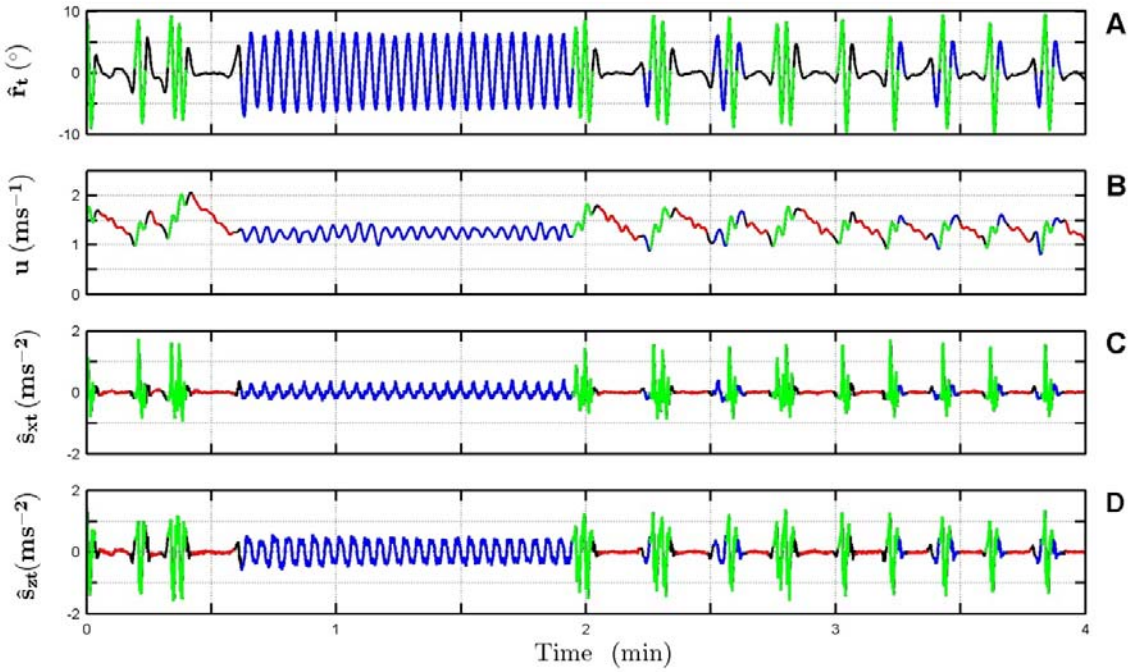

Figure 5. Estimated body rotations $\hat{r}_t$ (A), and forward speed u (B) compared to surge $\hat{s}_{xt}$ (C) and heave $\hat{s}_{zt}$ (D) accelerations during a *Ziphius* (Zc05_167a) steep (>40 degrees) ascent period. Speed was calculated from the vertical speed divided by the sin(pitch) sampled at 25 Hz, and was then smoothed with a low pass filter of 0.6Hz. Gliding periods, normal and B strokes are coloured red, blue and green respectively. The timing of strokes is taken from the rotation signal,$\hat{r}_t$.

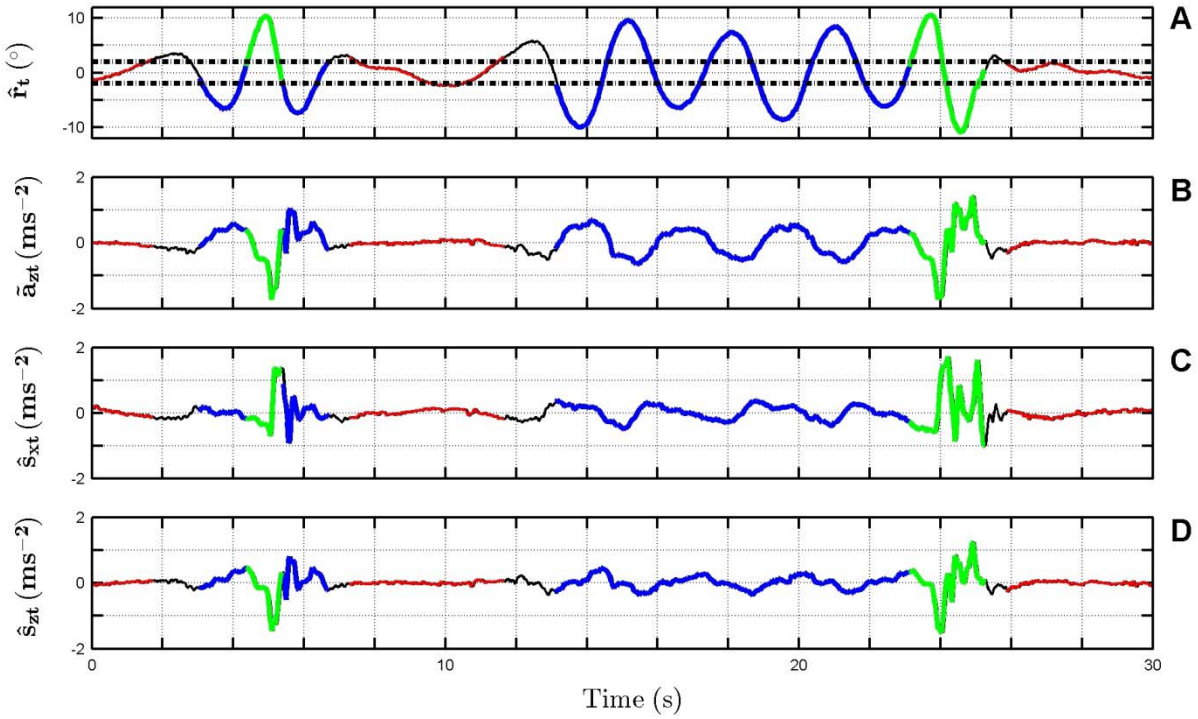

Figure 6. Detailed view of ascent fluking by a *Mesoplodon* (MdH1-03) showing the typical mixed gait comprising normal half-strokes (blue), B-half-strokes (green) and glides (red). (A) Body rotation $\hat{r}_t$. Dashed line represents the threshold (+/-J) used to detect zero-crossings and to distinguish gliding intervals. (B) High frequency dorso-ventral acceleration, $\tilde{a}_{zt}$. (C) and (D): estimated surge and heave acceleration $\hat{s}_{xt}$ and $\hat{s}_{zt}$, respectively in m/s^2. Glides are shown in red. Uncoloured periods are transition periods between glides and stroking which were not analysed. At this tag location (approximately midway between blow-hole and dorsal fin), surge and heave acceleration are some 90 degrees out of phase with body rotation with positive surge peaks occurring as the body at the tag position rotates through zero in a downwards direction. B-strokes sometimes appear as a single half-stroke (e.g., second 5) with just one large peak in surge and heave acceleration but others as a full stroke (e.g., second 24).